

1

Basic Electromagnetic Theory of SERS

Pablo G. Etchegoin and Eric C. Le Ru

1.1

Introduction

This chapter is aimed at introducing the newcomer to the field of surface-enhanced Raman spectroscopy (SERS), and is not intended to supplant the already available exhaustive literature in the field either in the form of review articles [1, 2] or books [3, 4]. As a technique, SERS is relatively exposed to the dangers of specialization due to its (intrinsic) multidisciplinary nature. The technique is becoming widespread and is finding new and exciting horizons in analytical chemistry [5–7], biology and biotechnology [8–12], forensic science [13, 14] and in the study of artistic objects [15–17]. While this is in many ways an advantage, it is also a handicap in the sense that scientists approaching the technique from a more ‘biological’ or ‘applied’ aspect might not have the appropriate background (or predisposition) to venture into the depths of electromagnetic theory and to understand the basic concepts of the theory of plasmon resonances in metallic nanostructures. This could be particularly true for students in the biotechnology field, who might find it desirable to have access to the elementary concepts (with a bare minimum of mathematics) but with enough insight to understand what they are actually doing in the lab. We believe that the success and use of the technique – in an environment which is by nature multidisciplinary – will be more effective if accessible presentations of the basic principles aimed at broader audiences are available at all times (and reviewed over prudent periods of time). This chapter (hopefully) fulfils part of that requirement.

This chapter is organized as follows: in Section 1.2, we introduce the basic principles of plasmon resonances and their associated field enhancements. Section 1.3, on the other hand, looks at the field enhancement distribution and localization produced by these plasmon resonances, while Sections 1.4 and 1.5 study the origin of the enhancement factor (EF) and its characteristic magnitude. Finally, Section 1.6 presents some conclusions and summarizes several main concepts.

1.2

Plasmon Resonances and Field Enhancements

1.2.1

Optical Properties of Simple Metals

None of the modern optical techniques such as surface-enhanced fluorescence (SEF) [18–20], surface plasmon resonance spectroscopy [21–23] or SERS itself [1, 4] would exist without the particular optical properties of *coinage metals* (with silver (Ag) and gold (Au) standing out as the most useful ones). The first obvious question is then what is it that makes the optical properties of metals so interesting? Hence, it is worth spending a few paragraphs on the topic of the optical properties of *bulk metals* such as Ag and Au to understand why they are so interesting, and why we use them in the aforementioned techniques.

The optical properties of bulk materials are characterized by their *dielectric function* $\epsilon(\omega)$. Most students from scientific disciplines would have come across the related *index of refraction* $n(\omega)$, which is linked to the former by $n(\omega) = \sqrt{\epsilon(\omega)}$. Both $n(\omega)$ and $\epsilon(\omega)$ depend on the frequency (ω) of the light (with $\omega = 2\pi c/\lambda$, where c is the speed of light and λ the wavelength), due to the fact that most materials respond differently to electromagnetic waves at different frequencies (wavelengths). The dielectric function can therefore be considered indistinctly as either a function of ω ($\epsilon(\omega)$) or λ ($\epsilon(\lambda)$). We shall use one or the other according to convenience. In the most elementary treatments of the optics of material objects (lenses, prisms, etc.) [24], both the dielectric function and the index of refraction are *positive real numbers* (more precisely ϵ , $n \geq 1$). More often than not, however, the dielectric function of materials at a given wavelength will be a *complex* (rather than real) number, and the material will not be transparent. In fact, this is more the rule than the exception, since the list of transparent materials constitutes a really small fraction of the materials we see around us. Metals are amongst the list of materials in which $\epsilon(\omega)$ is complex. The ultimate reason for the optical properties of materials is their *electronic structure*, and this is a canonical topic in solid-state theory [25, 26]. We shall not dwell too much on the details of the connection between the dielectric function of metals and their electronic structure (see Appendix D of Ref. [4] for a slightly more in-depth discussion), but rather take the properties of $\epsilon(\omega)$ of metals as given.

Figure 1.1 shows the dielectric functions of Ag and Au with their real and imaginary parts spanning from the near-UV (~ 300 nm) to the near-IR (NIR) range (~ 900 nm). These are analytical representations that interpolate rather well a collection of experimental results for $\epsilon(\lambda)$ obtained with different techniques. The accuracy and limitations of these fits are discussed in more detail in Refs. [4, 27]; here, we shall take these results as the starting point of our discussion on why the optical properties of metals are interesting. The main characteristics of the real and imaginary parts of the bulk $\epsilon(\lambda)$ for both metals can be summarized as follows:

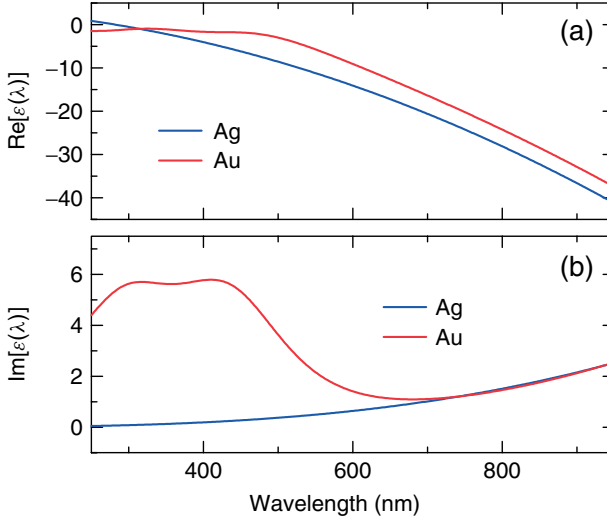


Figure 1.1 The real (a) and imaginary (b) parts of $\epsilon(\lambda)$ for the two most useful metals in SERS; that is, Ag and Au. Note the different vertical scales in (a) and (b); the imaginary parts of $\epsilon(\lambda)$ span over a smaller range and they are always *positive*. The real parts are *negative* across the visible range

(~400–750 nm) and show the overall (expected) characteristic of the simplest description of the dielectric function of metals (the lossless Drude model [25]), which predicts a $\sim -\lambda^2$ dependence for real part of $\epsilon(\lambda)$ at long wavelengths. See the text and Ref. [4] for further details.

- The real part of the dielectric function of both metals, for most of the visible range, is both *large* (in magnitude) and *negative*. *Later, this will turn out to be one of the most important properties of these metals* as far as their optical properties are concerned, and one of the main reasons for their usefulness as plasmonic materials. Furthermore, ignoring the imaginary parts of $\epsilon(\lambda)$ momentarily, we can claim that the real parts follow at long wavelengths one of the simplest models for the dielectric function of a (lossless) metal, which is the *lossless Drude model*. The latter predicts a dielectric function of the form [4, 25, 26]:

$$\epsilon = \epsilon_\infty \left(1 - \frac{\omega_p^2}{\omega^2} \right) = \epsilon_\infty \left(1 - \frac{\lambda^2}{\lambda_p^2} \right) \quad (1.1)$$

where $\omega_p = 2\pi c/\lambda_p$ is the so-called *plasma frequency*¹⁾ of the metal (proportional to the square root of the density of free electrons in it). The first expression on the right-hand side in Equation (1.1) holds if we want to express the dielectric function ϵ as a function of ω , while the last expression holds if ϵ is expressed as a function of $\lambda (= 2\pi c/\omega)$. Figure 1.1a reveals that both Ag and Au have actually very similar electronic densities, since the real parts of their dielectric functions are not too far away from each other. This is the approximate quadratic

1) For both Au and Ag, $\lambda_p = 2\pi c/\omega_p$ is around ~280 nm; that is, in the UV range.

downturn of the real part of $\epsilon(\lambda)$ seen in Figure 1.1a for longer wavelengths. We can see that, to a good approximation, the simplest lossless Drude model describes already a good fraction of the experimental results for the real parts seen in Figure 1.1a.

- Real bulk metals are *not* lossless, and this is where the imaginary part of $\epsilon(\lambda)$ comes into play. Even though when the $\text{Im}[\epsilon(\lambda)]$ for both metals are smaller than their real counterparts for most of the visible range, their effects are important and – in some cases – crucial. The imaginary part is always related to the *absorption* of the material (a material with $\text{Im}[\epsilon(\lambda)] = 0$ does not absorb light, and has a real index of refraction $n(\lambda) = \sqrt{\text{Re}[\epsilon(\lambda)]}$). It turns out that the imaginary part of $\epsilon(\lambda)$ for Ag can be obtained by a relatively easy generalization of the lossless Drude model (Equation 1.1). For Au, the situation is slightly more complicated; $\epsilon(\lambda)$ has additional contributions (in addition to that from the free electrons) from other electronic transitions in its electronic band structure [27]. This is the reason for the relatively higher absorption of Au (with respect to Ag) for $\lambda \leq 600$ nm, with a ‘double hump’ structure in the imaginary part (~ 400 nm), which comes from the so-called interband electronic transitions. Note, however, that for $\lambda \geq 600$ nm, the imaginary parts of $\epsilon(\lambda)$ for both Ag and Au become completely comparable (Figure 1.1b) and – with their real parts being comparable too in this range – both materials are similar (from the viewpoint of their electromagnetic response). Their surface chemistries are of course different, and one material might be preferred over the other for specific chemical reasons. But, as far as the electromagnetic response is concerned, Au is comparable to Ag in the near- and far-IR range.

1.2.2

Planar Surfaces

Once the complex dielectric function $\epsilon(\lambda)$ is known, all the electromagnetic properties of the material can be calculated in different geometries. The normal reflectance R (in the direction perpendicular to the surface) arises as a natural consequence of matching the boundary conditions of the fields at the interface.²⁾ The reflectance is plotted for Ag and Au in Figure 1.2b using the complex dielectric functions shown in Figure 1.1a and b. Silver has a very high reflectivity $\sim 100\%$ across the entire visible range. Gold, on the contrary, has $\sim 50\%$ for $\lambda \leq 600$ nm (from the yellow-green region towards shorter wavelengths in the UV). This is the reason for the ‘yellowish/reddish’ colour of flat gold when compared to silver. The overall high reflectivity of Ag does not come as a surprise; this is the reason why Ag

2) The standard boundary conditions for all electromagnetic problems require that the components of the electric field *parallel* to the surface (on both sides of the interface) are equal, as well as the *perpendicular* components of the displacement vector

$\mathbf{D} = \epsilon(\lambda)\mathbf{E}$. In standard notation [4, 28, 29] for an interface between medium 1 and 2: $E_1^{\parallel} = E_2^{\parallel}$, and $\epsilon_1(\lambda)E_1^{\perp} = \epsilon_2(\lambda)E_2^{\perp}$. The normal reflectance at a planar surface between the two media is given by $R = |(n_2 - n_1)/(n_2 + n_1)|^2$, with $n_1 = \sqrt{\epsilon_1}$ and $n_2 = \sqrt{\epsilon_2}$.

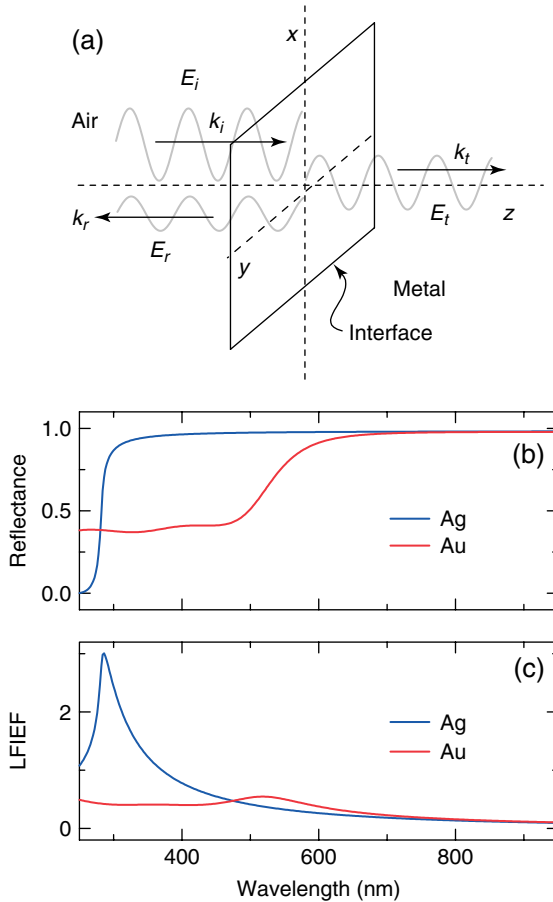


Figure 1.2 (a) An incident electromagnetic wave (with electric field E_i and wavevector k_i) impinges from the left (along z) onto a sharp interface with a (bulk) metal lying in the x - y plane, and transmitted and reflected waves result. The amplitude of the reflected (E_r) and transmitted (E_t) waves result from the matching of boundary conditions for the field at the interface, and depend only on the (complex) index of refraction of the metal ($n = \sqrt{\epsilon(\lambda)}$) [4, 28, 29]. (b) Reflectance at normal incidence for Au

and Ag, using the dielectric functions shown in Figure 1.1. Note that Ag has a reflectance close to $\sim 100\%$ across the entire visible range, while for Au the reflectivity decreases from ~ 500 nm towards the UV range.

(c) Local field intensity enhancement factor (LFIEF) at the surface of the metal [$(x$ - y) plane] for Au and Ag (at normal incidence). Note that, in general, the LFIEF is < 1 across the visible, meaning that the intensity is typically 'quenched' at the (flat) surface of the metal.

is used as a mirror in the visible. Gold mirrors, on the other hand, are preferred for NIR applications where it reflects as much as Ag, but it is more stable with respect to effects caused by long-term exposure to ambient conditions.

Another aspect of interest, while we dwell on the simplest of examples, is the Local Field Intensity Enhancement Factor (LFIEF) at the surface (i.e. by how much

the intensity of the electromagnetic field is changed with respect to the intensity we would have had at the place without the metal). The local field intensity at a specific point is proportional to the square of the electric field amplitude at that point: $|E(r)|^2$.³⁾ The LFIEF at a specific point is then the normalized value of $|E(r)|^2$ with respect to the intensity of the incoming field at that point: $|E_0(r)|^2$. Explicitly,

$$\text{LFIEF}(r) = |E(r)|^2/|E_0(r)|^2 \quad (1.2)$$

The LFIEF is, therefore, an adimensional magnitude expressing the (normalized) change in local intensity at a specific point produced by the presence of objects (which perturb the electric field of the light). Any optical technique that depends on the intensity of the light at a specific point will hence be linked to the LFIEF and, in general, depending on whether the LFIEF is >1 or <1 the optical process involved will be enhanced or quenched. The LFIEF will also depend on ω (or, equivalently, on λ), simply because the local field at a specific point depends on ω . We can formally write

$$\text{LFIEF}(r, \omega) = |E(r, \omega)|^2/|E_0(r, \omega)|^2 \quad (1.3)$$

In general, however, we will simplify the notation and emphasize only the most important dependence for the explanation of a specific aspect. We will refer, for example, to the LFIEF at a well-specified point in a geometry and at given frequency ω simply as LFIEF(ω).

The LFIEF at a flat surface for normal incidence (which results from the interference between E_i and E_r on the surface, see Figure 1.2) is another aspect of the classical problems in basic electromagnetic theory (and optics) [4, 28, 29], and (like R) is solely determined by ϵ_1 and ϵ_2 .

The LFIEF on the surface – for both an interface of Ag and Au with air – are plotted in Figure 1.2c.⁴⁾ As can be appreciated, the LFIEF is in general for normal incidence <1 at the surface of a planar interface separating a bulk metal (like Au or Ag) from air; that is, the intensity is ‘quenched’ at the surface compared to what we would have had in its absence. An ideal (100%-reflective) lossless metal will create a field on the surface, which cancels exactly the incoming one ($(E_i + E_r) = 0$), thus cancelling exactly the transmitted field too ($E_t = 0$) and sending the impinging electromagnetic wave back in the opposite direction from where it came. Therefore, a low LFIEF at the surface (achieved by the condition $E_i \sim -E_r$) is a natural consequence of having a very high reflectivity. In reality, the cancellation is not complete, but it is efficient enough to guarantee a low LFIEF on the surface and a concomitant high reflectance. The LFIEF is only >1 for Ag when $\lambda \leq 400$ nm, but this is the region where it actually stops being a good reflector. Larger (but, nevertheless moderate) LFIEFs may also be obtained at other angles of incidence (different from normal incidence shown here) and it is then also dependent on the incident polarization [4]. The reflection process for an arbitrary angle of incidence

3) We shall avoid vector notations throughout for simplicity.

4) The LFIEF immediately above the flat surface for normal incidence is given by

$$\text{LFIEF} = \left| \frac{4n_1}{n_1 + n_2} \right|^2 [4, 28, 29], \text{ where (as before) } n_1 = \sqrt{\epsilon_1} \text{ and } n_2 = \sqrt{\epsilon_2}.$$

and arbitrary polarization results in Fresnel formulas, which is (again) another aspect of the classic topics in the basic electromagnetic theory of optics [4, 28, 29].

It might appear up to this point that metals do not present any major advantage with respect to other types of materials as far as SERS is concerned. Except for their highly reflective properties (most familiar to everybody), it appears that molecules spread over a flat interface on the metal will not have much to win in terms of surface enhancement of the electromagnetic field. The key point to the usefulness of metals as photonic materials starts once we start considering the effects of *shapes*. This is the subject of the next section.

1.2.3

The Metallic Cylinder (2D) and Sphere (3D)

Let us consider now a different problem; the case of a (long) metallic rod (Au or Ag) embedded in a non-absorbing dielectric medium (with $\epsilon_M \geq 1$) being impinged by an electromagnetic wave of wavelength λ with polarization E_i perpendicular to the main axis of the rod. For all practical purposes, we can consider the problem to be two dimensional (2D) as shown in Figure 1.3a, for as long as the aspect ratio of the cylinder (basically its length divided by its diameter) is $\gg 1$.

1.2.3.1 The Electrostatic Approximation

If we want to know what happens to the electromagnetic field around the cylinder now, we have no other option but to actually solve Maxwell's equations subject to appropriate boundary conditions. This can be, in general, a rather difficult undertaking [4, 28, 29]. Full analytical solutions of Maxwell's equations exist in a handful of simple geometries, and these are useful to underpin basic concepts and ideas. More often than not, however, one has to resort to numerical solutions within some approximation scheme [4, 28, 29].

One useful approximation scheme – widely used in the literature – is the *electrostatic approximation*, explained in full detail in Refs. [4, 30]. This is schematically represented in Figure 1.3b for the aforementioned cylinder. In this approximation, the problem is solved as in electrostatics, but at different ω 's (λ 's) using the complex dielectric function of the material at that frequency (wavelength). Accordingly, we solve in this case *Poisson's equation* for the electrostatic field. This is much easier than solving Maxwell's equations in full, for it involves only an equation for the scalar electric potential $\phi(\mathbf{r})$. Nevertheless, at the time of satisfying boundary conditions we do use the complex dielectric function $\epsilon(\lambda)$.

The electrostatic approximation corresponds then to ignoring the presence of the wavevector k (or, equivalently, the wavelength $\lambda = 2\pi/k$) in Figure 1.3a. The applied electric field does not have a 'wavelength', therefore, but rather it is a uniform field oscillating up and down with frequency ω . Obviously, this is an approximation and it is bound to fail in many cases. It is not too difficult to imagine that the electrostatic approximation works well when the size of the object is much smaller than the wavelength. In this case, the electric field of the light will be in any case

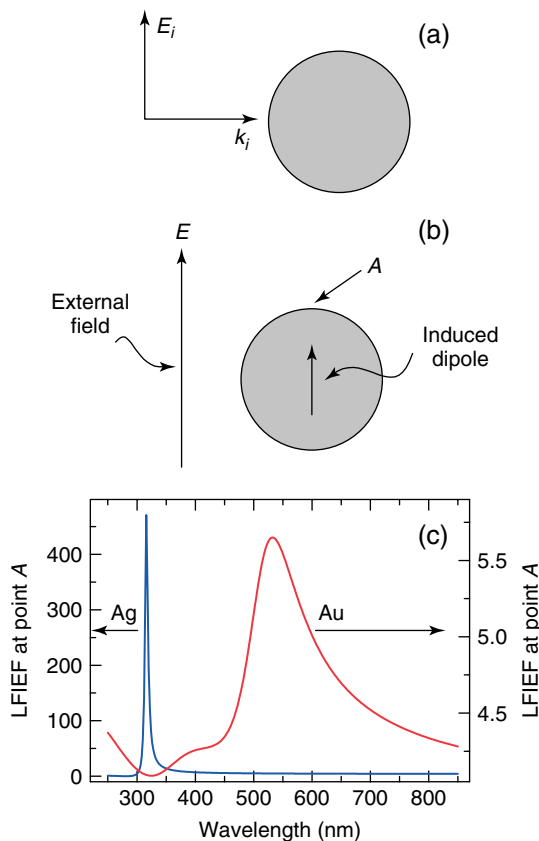


Figure 1.3 (a) A cylindrical metallic object is impinged by an electromagnetic wave coming from the side with wavevector k_i and polarization E_i (on the plane of the page). (b) When the object is small compared to the wavelength ($\leq 10\text{--}20$ nm), it is possible to gain some insight into the situation by solving the problem *electrostatically* [4, 30] (i.e. in a constant electric field in the direction of the polarization and with no wavevector present). The boundary conditions at different wavelengths ($\lambda = 2\pi c/\omega$) are still specified by $\epsilon(\lambda)$, and can be fulfilled exactly

at the surface of the cylinder by considering the superposition of an *induced dipole* and the external field (Equation 1.4). (c) The local field intensity enhancement factor (LFIEF) at point A (immediately above the surface) for Ag or Au cylinder and for different wavelengths. Note the different scales for Au and Ag in (c). Silver achieves a much higher LFIEF (at a much shorter wavelength). This is due to the much less absorption of Ag compared to Au in the place where the resonance condition for a cylinder is achieved: $\text{Re}[\epsilon(\lambda)] = -1$ in air.

approximately constant over distances comparable to the size of the object, and it will look like a uniform field oscillating up and down at a frequency ω . In practice – with typical wavelengths in the visible being in the range $\sim 500\text{--}600$ nm – it means that the electrostatic approximation will be mostly valid for objects of typical sizes in the range of ~ 10 nm or smaller. However, it is sometimes used for even larger objects and, in some cases, in limits where it would be clearly invalid [30].

With these limitations in mind, it is always possible to use the electrostatic approximation for *nano-optics* and, indeed, it gives truly valuable insights into the electromagnetic properties of many systems of interest and (more than that) yardstick values for LFIEFs.

1.2.3.2 Localized Surface Plasmon Resonances of the Cylinder

The exact electrostatic solution of a 2D cylinder with dielectric function $\epsilon(\lambda)$ turns out to be analytically tractable. It turns out that boundary conditions on the surface of the cylinder can be *exactly* satisfied by considering the superposition of the external field E with an *induced dipole* centred at the origin, as depicted in Figure 1.3b. As far as points outside the cylinder is concerned then, the electric field looks like the superposition of this dipole (p) at the origin and the external field. We shall not go into the details of the solution of the electrostatic problem to keep the mathematical aspects to a bare minimum, but rather only mention that the magnitude of the induced dipole that satisfies the boundary conditions and solves the electrostatic problem is proportional to

$$p \propto \left(\frac{\epsilon(\lambda) - \epsilon_M}{\epsilon(\lambda) + \epsilon_M} \right) \quad (1.4)$$

Dipoles in 2D are more complicated than standard dipoles in 3D. Note that it should be described more formally as a ‘dipolar line’ (in the direction perpendicular to the page as shown in Figure 1.3) rather than a dipole. The 2D solution has certain peculiarities that we are not going to analyse in detail here, but rather concentrate on a few salient aspects. The most important detail of the proportionality in Equation 1.4 is the presence of the denominator ($\epsilon(\lambda) + \epsilon_M$). With $\epsilon(\lambda)$ being a complex number, it is obviously not possible to satisfy in full the condition $\epsilon(\lambda) = -\epsilon_M$ exactly (which would imply $p \rightarrow \infty$). But it is evident, at the same time, that an interesting situation will happen when the real part, at least, satisfies the condition $\text{Re}[\epsilon(\lambda)] = -\epsilon_M$; in particular, if the imaginary part of $\text{Im}[\epsilon(\lambda)]$ at that λ is small. This is, indeed, the case for metals (with Ag being a better example of this than Au). At the wavelength where $\text{Re}[\epsilon(\lambda)] = -\epsilon_M$, the magnitude of p will only be limited by how small the imaginary part of $\epsilon(\lambda)$ is, and this will show as a *resonance* (i.e. a large response of the system), called the dipolar localized surface plasmon (LSP) resonance of the cylinder. A very important point to note here is that this resonance is *purely induced by geometrical aspects* (i.e. the shape of the object, a cylinder in this case), and the fact that we need to satisfy boundary conditions. The denominator ($\epsilon(\lambda) + \epsilon_M$) is purely a consequence of satisfying the specific boundary conditions for this particular geometry (a cylinder). Note, however, that the condition $\text{Re}[\epsilon(\lambda)] = -\epsilon_M$ introduces a small dependence of the resonance wavelength on the embedding medium (characterized by ϵ_M). As a result, the LSP resonance is red shifted in media with a larger ϵ_M (for example, in water compared to air).

Objects with different shapes will have different resonances (sometimes more than one), and this is one of the most important properties why metals are so interesting for nano-optics. The fact that metals have negative $\text{Re}[\epsilon(\lambda)]$ spanning a wide range in magnitude from $\text{Re}[\epsilon(\lambda)] \sim 0$ when $\lambda \sim \lambda_p$ (Equation 1.1) to very

large (and negative) values when $\lambda \rightarrow \infty$ ($\omega \rightarrow 0$, see Figure 1.1) makes them ideal to satisfy a wide range of *resonance conditions* that appear in the solutions of the electromagnetic responses of many objects. The latter is aided by the fact that these conditions for the real part happen at λ 's where $\text{Im}[\epsilon(\lambda)]$ is either small or at least not too large (Figure 1.1). Geometry-induced resonances are at the heart of plasmonics and the usefulness of coinage metals.

1.2.3.3 Localized Surface Plasmon Resonances of the Sphere

We give an additional example to show how the resonance changes with geometry with the standard case of the *metallic sphere* in Figure 1.4. The sphere is one of the problems where we can still resort to exact solutions of Maxwell's equations (Mie theory [4]) or approximate (electrostatic approximation) solutions of the electromagnetic problem. It has been treated in full detail in the literature [4] and we, therefore, only mention here some essential aspects in the simplest of approximations. As before (for the cylinder) the electrostatic problem of a sphere in a uniform field can be solved analytically [28, 29]. It turns out that (as in the case of the cylinder) the electrostatic boundary conditions on the sphere can be satisfied *exactly* by considering the superposition of an induced dipole at the origin p with the external applied field E . However, the magnitude of the induced dipole is now (in the 3D problem) proportional to

$$p \propto \left(\frac{\epsilon(\lambda) - \epsilon_M}{\epsilon(\lambda) + 2\epsilon_M} \right) \quad (1.5)$$

The most important change with respect to the previous case is the fact that the resonance condition in the denominator has changed to $\epsilon(\lambda) = -2\epsilon_M$. As before, however, this condition cannot be satisfied exactly because of the presence

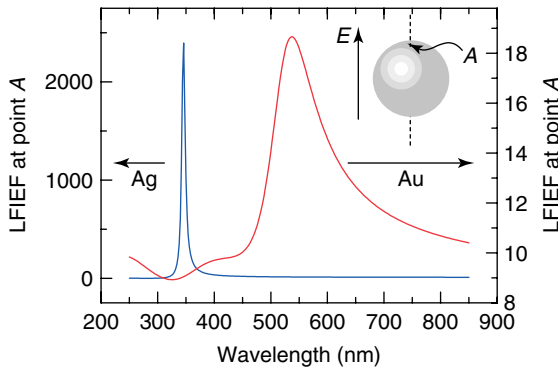


Figure 1.4 Local field intensity enhancement factor (LFIEF) at point A (inset) on a sphere of either Au or Ag in the electrostatic approximation [4, 30]. The points of largest LFIEFs on the surface are along the main symmetry axis in the direction defined by the polarization of the electric field E . Note

that maximum LFIEFs are higher than in the case of cylinders from the same materials (Figure 1.3c) and also that the maxima of the LFIEFs happen at slightly different frequencies; accounting for a different resonance condition (with respect to cylinders) given by $\text{Re}[\epsilon(\lambda)] = -2$ (Equation 1.5) in air.

of the imaginary part of $\epsilon(\lambda)$, but a shape-induced resonance condition will arise when $\text{Re}[\epsilon(\lambda)] = -2\epsilon_M$ and will be limited only by how small $\text{Im}[\epsilon(\lambda)]$ is at that particular λ .

1.2.3.4 Local Field Enhancements

On the surface of the sphere, the places with the largest local fields are the two points along the axis that goes through the centre of the sphere, and is oriented in the direction of the external field (one of them labeled as ‘point A’ in Figure 1.4). This can be easily understood if we look at the superposition of the induced dipole and the external field, for these are the two points where the two add up (on the surface) in the same direction. In 2D (because of the peculiarities of dipoles in two dimensions) it turns out that the intensity is constant over the surface of the cylinder! We still evaluate, though, the intensity at one point on the surface (also labeled as point A in Figure 1.3b). In Figure 1.3c, we calculate LFIEF at point A as a function of wavelength for the dielectric functions of Ag and Au (given in Figure 1.1). Note the different scales (on the left and right) in Figure 1.3c for the Ag or Au cases. The LFIEF then tells us how bigger or smaller the intensity at point A (Figure 1.3b) will be due to the presence of the cylinder. This would be the *intensity enhancement* that a molecule would experience if it were located at that position. As can be appreciated from Figure 1.3c, the individual LFIEFs have a characteristic peak. This peak appears at the wavelength λ where the condition $\text{Re}[\epsilon(\lambda)] = -\epsilon_M$ is satisfied (Figure 1.1). Ag has a stronger (and narrower) LFIEF resonance. This can be again easily understood by the fact that the condition $\text{Re}[\epsilon(\lambda)] = -\epsilon_M$ is satisfied in Ag at a wavelength λ where the imaginary part is much smaller (comparatively speaking) than that of Au at its corresponding resonance frequency. This makes the resonance in Au lossy and, accordingly, broad. An important concept to realize here is that these resonances happen at λ 's where there is no intrinsic feature (or peak) in the *bulk* dielectric function of the materials themselves. In other words, these resonances appear as purely *geometrical* aspects of the problem.

On the other hand, Figure 1.4 displays the LFIEF at point A on a sphere as a function of wavelength for Au and Ag. Figure 1.4 shows again the clear presence of resonance peaks where the LFIEF is large for both Ag or Au spheres. Note that the resonances occur at slightly different wavelengths from those in the 2D cylinder, accounting for the new resonance condition $\text{Re}[\epsilon(\lambda)] = -2\epsilon_M$ (instead of $\text{Re}[\epsilon(\lambda)] = -\epsilon_M$ for the cylinder). Note also that the LFIEFs are larger than in the case of the cylinder. In the case of Ag, a molecule sitting at point A on the sphere will experience (at resonance) more than three orders of magnitude intensity compared to what it would have experienced otherwise.

Despite their simplicity, these truly basic examples show already why plasmon resonances in metals are interesting and important. Intensities can be boosted by large factors and resonance can be ‘tuned’ by geometrical aspects of the problem. These two basic topics are further explored in the next section.

1.2.4

Size Effects

Note that in the electrostatic approximation, the problem becomes *scale invariant*; that is, it does not really matter what the actual size of the sphere is. If we increase or decrease the size of the sphere by a certain factor, the LFIEF will still be the same in the electrostatic approximation. Nevertheless, the conditions under which the electrostatic approximation will represent most faithfully the *real* solution of the problem (which is *not* electrostatic [4]) is when the size of the sphere is a few tens of nanometers (at most) in size. In all the examples, therefore, we always assume objects in the tens-of-nanometers size range, even though the actual solution of the problem is independent of this assumption.

But *size does matter*, and for objects in the range of typical dimension $\sim 30\text{--}100$ nm there will be, in general, size effects (see also Section 2.2.1.3). The fact that the size of the object is now a substantial fraction of the wavelength cannot be ignored anymore and the electrostatic approximation fails. The effect on the plasmon resonances of different sizes is very often really complicated to analyse in simple terms and relies mostly on the numerical solution of Maxwell's equations. But the size effects can be qualitatively summarized as follows:

- LSP resonances red shift as the size increases.
- LSP resonances are strongly damped as the size increases, mostly as a result of increased radiation losses. This results in the broadening of the resonance, and more importantly in a dramatic decrease in the associated LFIEF. The resonance (and any substantial LFIEF) ultimately disappears for large sizes, typically 100 nm for dipolar LSP in spheres, but possibly at larger sizes for other geometries.
- Another typical consequence of size is the appearance of resonances that do not exist in the small size limit (where the electrostatic approximation was sufficient). These 'new' size-related resonances (for a fixed shape) are typically related to the activation of *multipolar resonances* (with the quadrupolar resonance playing typically the most important role) that do not couple to light very effectively in the limit of small sizes. Size-induced resonances add yet another layer to the diversity (and complexity) of optical phenomena in metallic nanostructures.

1.2.5

Shape Effects

The two examples given earlier highlight the concept of *geometry-induced resonance* which is a defining characteristic of LSP resonances in metallic nanostructures (see also Section 2.2.4). The obvious question that now arises is what happens with other geometries? Unfortunately, a rule of thumb is that the simplest examples of geometries are at the same time the *only* ones that can be typically solved analytically. Except for a handful of exceptions, even some of the simplest geometries beyond cylinders and spheres (like triangular shapes or prisms) are not analytically soluble (not even in the electrostatic approximation). Numerical solutions come here as an

aid to these cases and, as a rule of thumb, we have no option but to resort to them in order to obtain the solution of the electromagnetic problem.

Figure 1.5 shows an example of shape-induced resonances for a 2D shape with a triangular cross section. Figure 1.5a and b shows the spatial distribution of the LFIEF at two different wavelengths, while Figure 1.5c shows the spectral dependence of the LFIEF on the surface at two different points (labeled *A* and *B* in Figure 1.5a and b). Note that in an equilateral triangle all vertices are, in principle, equivalent, but the presence of an electric field in the vertical direction in this case breaks the symmetry of the problem and makes points like *A* and *B* in Figure 1.5a and b inequivalent. Figure 1.5c shows the spectral (wavelength) dependence of the LFIEF at points *A* and *B* (on the surface) of the triangular shape. The problem was solved numerically in the electrostatic approximation [4]. A few obvious conclusions arise from the calculation in Figure 1.5c:

- Unlike what happens in the examples of the cylinder and the sphere, there will be, in general, more than one resonance condition associated with a given shape. Some of these resonances have complicated spatial distributions of the enhancement.
- Different points on the surface can have their maximum LFIEFs at different wavelengths (as it is the case for points *A* and *B* in Figure 1.5a and b). The LFIEF is strongly position dependent in most cases.
- The maxima of the LFIEFs shown in Figure 1.5a and b are simple examples of what is normally dubbed as *the lightning rod effect* (i.e. electric fields concentrating at sharp ends). One should keep in mind though that the real lightning rod effect makes reference to a truly electrostatic situation ($\omega = 0$, or $\lambda = +\infty$), while the cases shown in Figure 1.5a and b are resonances that occur at frequencies in the visible range ($\omega \sim 10^{15}$ Hz).
- The LFIEF in more complicated shapes than the simplest cases of the cylinder or sphere can be really high in some circumstances (in particular, if the shape has sharp corners as in Figure 1.5). In the specific case of the triangular shape, the LFIEF at point *B* felt by a molecule can achieve (at its maximum) well over four orders of magnitude the intensity it would have felt if it had been in free space under the influence of the same field.
- In general, the resonances (in their wavelength position and intensity) will depend not only on the shape but also on the orientation with respect to the field. If the direction of the electric field is changed in Figure 1.5 while keeping the triangular shape in the same position, the LFIEFs at points *A* and *B* will change accordingly (in both intensity and frequency position). In the *real* solution of the electromagnetic problem (not in the electrostatic approximation), there is also the direction imposed by the wavevector of the light k . While the latter has in general less importance than the direction of E (in particular, for really small objects of the order of ~ 10 nm in size), there are many subtle details of the electromagnetic field distribution that does depend on it.

The dependence of the LFIEFs on shape and polarization/wavevector directions is what gives plasmon resonances in metallic nano-objects their vast richness and

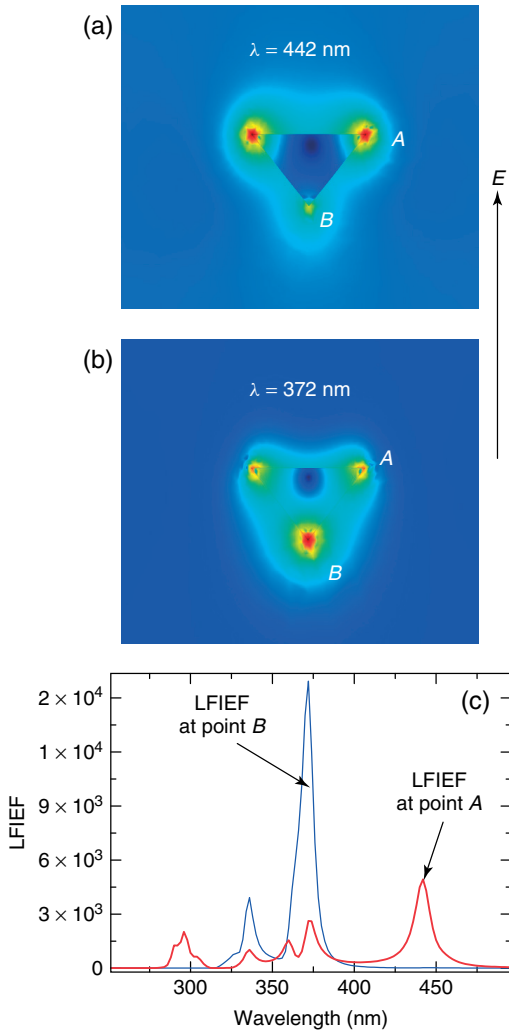


Figure 1.5 Local field intensity enhancement factor (LFIEF) at two different wavelengths for a triangular Ag shape in the electrostatic approximation. The direction of the polarization is vertical. The LFIEF is shown at two different wavelengths: (a) 442 nm and (b) 372 nm, where the highest LFIEFs occur at points A and B, respectively. The plots are in a logarithmic (false) colour scale, where red is the highest and blue the lowest. The wavelength dependence of the LFIEF at A and B is shown in c. These are examples of shape-induced resonances, affecting the

enhancement factor at different points on the surface of the shape. Note that point A achieves the maximum LFIEF at a different wavelength from point B. Even when the triangular cross section is equilateral and all vertices are equivalent, the electric field breaks the symmetry of the problem and points A and B are no longer equivalent. The resonances at A and B are simple examples of the ‘lightning rod effect’ in the optical range (see the field distribution in (a) and (b)).

complex variety of phenomena. In addition, once interactions among objects are introduced and the concept of coupled plasmon resonances appears, these are *not* the only factors that can produce them.

1.2.6

Interacting Objects and Gaps

1.2.6.1 Coupled Plasmon Resonances

The induced dipoles appearing in the cylinder and sphere cases (Figures 1.3 and 1.4) provide the necessary mind frame to introduce another extremely important effect in the metallic nanostructures; to wit, the existence of *coupled plasmon resonances* for two or more closely spaced objects (see also Sections 2.2.2 and 2.4). We give a somewhat oversimplified description here emphasizing the qualitative aspects.

Imagine the presence of two (instead of one) cylinders, as depicted in Figure 1.6a. If the cylinders are far apart from each other (several diameters) they can be considered as two independent problems of single cylinders. However, as they approach each other, the field produced by their respective induced dipoles start to interact. This interaction can reinforce or weaken the field in certain regions of space. In a manner reminiscent of atomic orbital bonding in atoms (in the H_2 molecule, for example), the interaction of the induced dipoles changes the spatial configuration of the fields (wavefunctions in the case of orbital bonding) and shifts the intrinsic energy of the resonances. In fact, something somewhat reminiscent of the creation of a *bonding* and anti-bonding resonance happens, with the ‘bonding’ resonance being concentrated in the middle of the two cylinders and being red shifted with respect to the individual (isolated) resonances at far distances. The analogy with orbital bonding is mostly semantic, for they are indeed very different problems. But it helps to understand the qualitative picture of interaction and red shifting of the resonance.

A much more complicated picture arises in the electromagnetic case though [31, 32], with resonances coming from higher-order multipoles being activated by the interaction. Be it as it may, the fact remains that there will be a red shifted plasmon resonance with its intensity mainly concentrated in the middle of the two cylinders, and that this *coupled resonance* comes (primarily) from the interaction of the induced dipoles in each individual cylinder. This can be illustrated by the examples in Figure 1.6b–d, where the LFIEF at the centre of the axis separating the two cylinders in Figure 1.6a is calculated for different separations (gaps). These results are of course limited by the validity of the electrostatic approximation, but the qualitative features do not change with more sophisticated methods. At a separation of 20 nm in Figure 1.6b, the interaction between the two cylinders is weak and we can still see the main individual resonance of the cylinders, slightly affected by the interaction with a small shoulder at shorter wavelengths. When the cylinders are drawn together, a clear red shift of the strongest peak (the dipolar interaction coupled plasmon resonance) can be seen. The strongest coupled plasmon resonance is indicated with an arrow in Figure 1.6b–d. Note that not only the resonance shifts but the LFIEF also becomes larger. At separations of

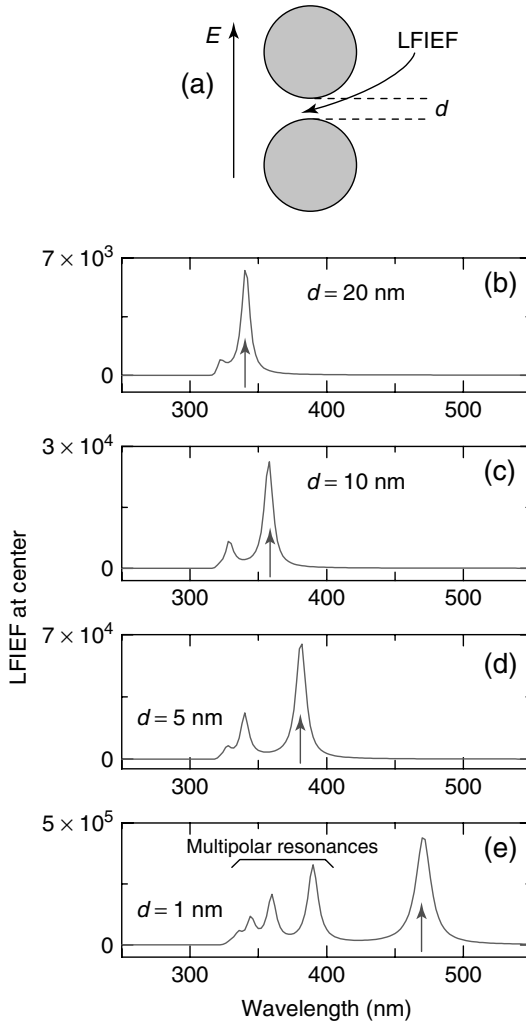


Figure 1.6 Gap effects: (a) the local field intensity enhancement factor (LFIIEF) at the centre of a dimer formed by two identical (50 nm radius) Ag metallic cylinders separated by a distance d and with the electric field pointing along the axis joining the two cylinders. The LFIIEF as a function of λ (in the electrostatic approximation) is plotted for different separations of (b) 20 nm, (c) 10 nm, (d) 5 nm, and (e) 1 nm. The peak labeled with an arrow is the interacting coupled (dipolar) plasmon resonance

between the two cylinders, which red shifts and increases the LFIIEF at the centre as the cylinders get closer (note the different vertical scales in (b)–(e)). The additional resonances contributing to the LFIIEF at shorter wavelengths (clearly visible in (e), for example) are higher-order multipolar resonances. Note that the maximum LFIIEF in (e) is about ~ 3 orders of magnitude larger than the maximum value for a single cylinder (Figure 1.3).

the order of ~ 1 nm, LFIEFs can reach (for Ag) values of the order of $\sim 10^5$. These values (when used within the framework of SERS) allow the observation of single molecules, as we shall discuss later. Note that SERS EF is approximately the square of the LFIEF, as explained later.

Coupled plasmon resonances provide some of the highest EFs for optical spectroscopy available. It is difficult to emphasize enough their importance in the fields of SERS and related technique. By the same token, they add an additional level of complexity to the phenomena described already in terms of shape and size. The complexity of plasmon resonances when the issues of shape, size, and interactions are included is enough to justify an entire field or research by itself: *plasmonics*. One of the main aims of plasmonics (and plasmonic engineering) is to precisely tailor-make and understand nanostructures that can benefit the most from plasmon resonances for applications in optical spectroscopy. Plasmonics (as a field) is, in fact, more general and does not only include the study of nanoparticles but also the properties of propagating plasmons, meta-materials, near-field effects, and so on.

1.2.6.2 Tip-Enhanced Raman Scattering (TERS)

Undoubtedly, a major breakthrough in SERS in the last few years has been the introduction of the related technique tip-enhanced Raman scattering (TERS) [33–35]. Needless to say, coupled plasmon resonances are not limited to gaps between objects with the same geometries, but rather exist (to a larger or lesser degree) for any pair of metallic interacting objects. A particularly important case of coupled plasmon resonances happens between a flat metallic surface and a tip, as displayed schematically in Figure 1.7. Metallic tips of different kinds can be used in this technique, thus opening (simultaneously) the possibility of combining TERS with other types of microscopy (AFM, STM, etc.). Figure 1.7 shows an example in the spirit of the previous cases studied in this chapter; that is, a calculation in the simplest case of the electrostatic approximation. If we set the external field direction along the axis of the tip (as actually shown in Figure 1.7), we are modelling an experimental situation often encountered in which the laser is delivered from the side at almost grazing incidence with the surface and with the polarization along the tip. This choice of electric field is due to the fact that this is the polarization that couples most efficiently to the plasmon resonance resulting from the interaction between the surface and the tip. Figure 1.7a shows a LFIEF map (in a false-colour log-scale) at 620 nm where the clear presence of a hot spot in between the tip and the surface can be seen. In Figure 1.7b, on the other hand, we show the LFIEF at point A (in Figure 1.7a) that is located ~ 0.5 nm away from the surface and directly below the tip. This is the position that a deposited molecule on the substrate (of typical size ~ 1 nm) would be occupying under the tip. As can be seen from Figure 1.7b, a clear coupled surface plasmon resonance develops under the tip. The position of the resonance (and its maximum LFIEF) can be tuned to some degree by both the geometrical aspects of the tip and the separation distance from the surface d . The latter can be very efficiently controlled, for TERS systems normally use piezo-controllers (of the same type used in AFM and STM) to position

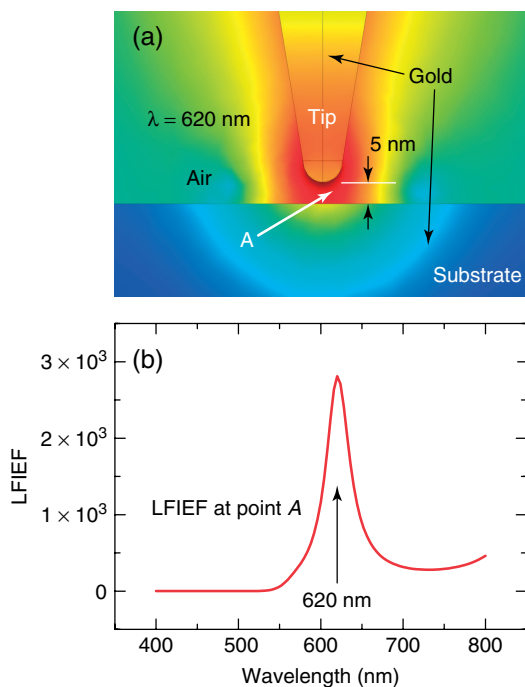


Figure 1.7 (a) A typical TERS geometry: a flat substrate and a tip (both made of gold in this case) are brought together with a gap of a few nanometers in between. The tip in this case has a conical body with a hemisphere termination (10 nm in diameter), and it is separated by 5 nm from the surface. A 3D simulation in the electrostatic approximation at 620 nm excitation (with the field E in the vertical direction) shows

the displayed LFIEF map (in a false-colour log-scale as shown in the previous figures). If we monitor the LFIEF for different λ 's at point A (which is 0.5 nm above the surface and immediately below the tip), we obtain the result displayed in (b). This would be approximately the position that could be occupied by a molecule lying on the surface. The peak at ~ 620 nm is the coupled plasmon resonance between the tip and the surface.

the tip and scan over the surface. TERS (and other tip-related techniques; see also Chapter 14) could be considered as a branch of SERS, even though it has a certain life of its own. In the last few years, impressive advances have been made on the technique from both experimental and theoretical aspects, as any brief detour into the current literature can demonstrate (see, for example, Refs. [33–38] to acquire a flavour of current topics in tip-related techniques).

1.2.7

Choice of Metal

1.2.7.1 Gold versus Silver

In the examples given above, it is clear that Ag outperforms Au in most cases, and this can be tracked down (ultimately) to the higher absorption (which is proportional

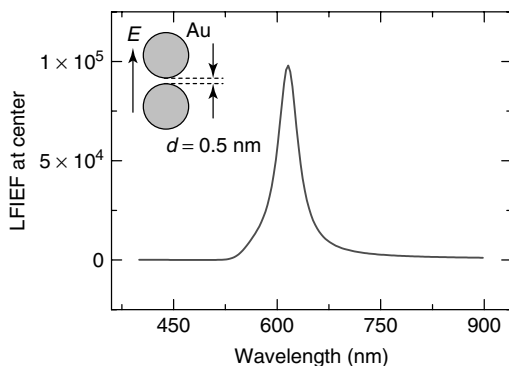


Figure 1.8 Local field intensity enhancement (LFIEF) caused by a coupled plasmon resonance at the centre of two 50 nm radius Au cylinders separated by a small gap of 0.5 nm. The coupled plasmon resonance is red shifted to a wavelength where the absorption of Au is comparable to that of Ag (see the comparison imaginary parts of $\epsilon(\lambda)$ in Figure 1.1(b)), thus achieving a maximum LFIEF which is comparable to those obtained in Ag. For coupled resonances in the red and NIR ($\lambda > 600$ nm), Au is as efficient as Ag for SERS applications and preferable in many cases due to its intrinsic stability, well-known surface chemistry, and biocompatibility.

to $\text{Im}[\epsilon(\lambda)]$) that Au has at the frequencies where the resonances occur. This is basically the origin of the results seen in Figures 1.3c and 1.4. However, the red shift induced by object interaction and/or shape-and-size effects can push the resonance in Au to the wavelength region $\lambda > 600$ nm, where (as can be seen in Figure 1.1) $\text{Im}[\epsilon(\lambda)]$ becomes comparable for both metals. In this case, *gold can be as good as silver* as far as LFIEFs are concerned. This is illustrated explicitly in Figure 1.8 for a coupled plasmon resonance in Au. Irrespective of the oversimplified nature of the example in Figure 1.8 (2D cylinders and electrostatic approximation), the fact remains that coupled plasmon resonances in Au nanostructures can be as efficient as those in Ag. In fact, the range $\lambda > 600$ nm is really important for many practical applications of SERS. Many biological [39] (and forensic) applications of the technique are based on NIR lasers (typical examples being diode lasers at ~ 750 or ~ 830 nm; see also Section 2.2.1.4). In biological applications, therefore, Au will probably be the most preferred plasmonic substrate (see also Chapters 12 and 13). To the fact that LFIEFs can be comparable to the best values in Ag, we add the advantage of the greater (chemical) stability of Au surfaces in the long run, and the better biocompatibility with many molecules of interest. Examples of EFs in Au comparable to the best values found in Ag have been extensively studied in the literature [4], with more realistic geometrical models for hot spots (a dimer of spheres, for example) and exact solutions (Mie theory) of the electromagnetic problem.

1.2.7.2 Other Coinage and Transition Metals

It is worth mentioning that other coinage metals (besides Ag and Au; see also Sections 2.2.1.1 and 2.2.3) can also be potentially used for enhancing

electromagnetic fields. The reason why they are not as useful as Ag and Au is mainly because of their specific dielectric functions [4]. For example, for aluminium (Al) [40, 41], in the region where $\text{Re}[\epsilon(\lambda)]$ is negative, – and can satisfy resonance conditions such as those imposed by Equations 1.4 and 1.5 – the imaginary part is at least an order of magnitude larger than that of Ag or Au, peaking at $\text{Im}[\epsilon(\lambda)] \sim 50$ at ~ 800 nm. Compared to Ag and Au, therefore, resonances experience a much larger damping and are broader and weaker. The use of other coinage metals and transition metals (Pt, Ru, Rh, Pd, Fe, Co and Ni and their alloys [42–44]) is sometimes pursued as an academic interest, but occasionally also as important substrates for specific applications (SERS in the UV range, for example).

1.3

Field Enhancement Distribution and Localization

1.3.1

Electromagnetic Hot Spots

The calculation shown in Figure 1.6 is an example of how the LFIEF can reach really high values ($\sim 10^5$) through coupled resonances at the ‘gaps’ between metallic nano-objects. These large enhancements are informally dubbed *hot spots* in the SERS literature. Hot spots play a fundamental role in techniques such as SERS, for they provide in many cases enough enhancement to detect single molecules [47, 48] (see also Chapter 4). But, there are other aspects associated with hot spots that are important and worth highlighting besides the magnitude of the LFIEF. The large increase in the LFIEF at hot spots is normally associated also with a strong *spatial localization* of the resonance in the gap. This effect has been studied in full detail in the specialized literature [4] with realistic geometries (a dimer of spheres, for example) and more sophisticated methods to solve Maxwell’s equations (generalized Mie theory [4], for example), but – as before – we shall provide here one of the simplest demonstrations with two cylinders in 2D in the electrostatic approximation. Figure 1.9a shows the spatial distribution of the LFIEF at 471 nm under the conditions used previously in Figure 1.6e. At 471 nm we are at the wavelength where the LFIEF is maximum due to the coupled (dipolar) plasmon resonance between the two cylinders in Figure 1.6e. As can be seen in Figure 1.9a, the LFIEF is highly localized in the gap separating the two cylinders (the LFIEF is represented in a false-colour logarithmic scale in Figure 1.9a). This is further reinforced by the data in Figure 1.9b, in which the LFIEF on the surface of the bottom cylinder is shown as a function of Θ . The intensity falls already by a factor of two when $\Theta \sim 2.66^\circ$ from the central axis. How much this actually represents in terms of distance along the surface of the cylinder depends on the radius of the cylinders, but a rule of thumb is that it is typically enough to move by a few nanometers (say ~ 5 nm) from the maximum LFIEF at a hot spot to have a decrease in the LFIEF by an order of magnitude (or more). This is a defining characteristic of the hot spots and one that results in a probability distribution of enhancements

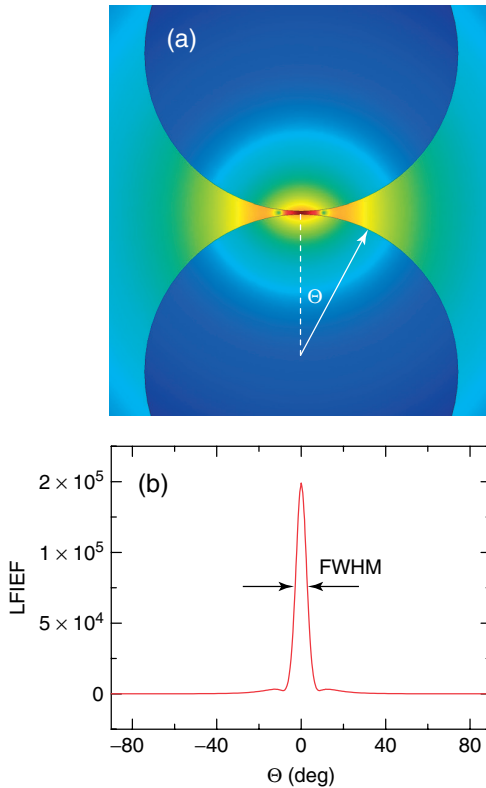


Figure 1.9 (a) Spatial distribution of the LFIEF between two (50 nm radius) Ag cylinders at 471 nm (the position of the peak labeled with an arrow in Figure 1.6e). The LFIEF is plotted in a logarithmic (false-colour) intensity scale with red being the most intense and blue being the weakest. The highly concentrated (in the gap) nature of the dipolar coupled plasmon resonance at 471 nm is clearly seen in the LFIEF map. Localized coupled plasmon resonances like this one are normally responsible for the so-called *hot spots* in SERS substrates.

Hot spots are highly localized regions in space. In (b) we show the angular variation of the LFIEF on the surface of the cylinder as a function of Θ . The LFIEF decays to half of the value at the maximum at $\Theta \sim 2.6^\circ$. In real (experimental) hot-spots used for single-molecule SERS, the intensity can decrease by an order of magnitude by moving a few nanometres from the maximum, thereby resulting in some extreme statistical behaviour that has been the topic of study (and of contradictions in the literature) for a very long time [45, 46].

that is *long tail*, for molecules randomly distributed on the surface of the metallic nano-objects.

1.3.2

Long-Tail Distribution of Enhancements

Imagine we have two metallic objects producing a hot spot at a gap (coupled plasmon resonance). For the sake of argument, let us take the example of a dimer

formed by two 30 nm in radius Au spheres separated from each other by a gap of 2 nm. As in all the previous examples, we can gain some insight into the problem by solving it within the electrostatic approximation. Let us further suppose that we take a typical experimental condition; for example, we are using a 633 nm laser (HeNe) to illuminate the dimer and we have molecules (randomly) distributed on the surface of the metallic spheres. A pertinent question at this point is then what is the probability of having a certain enhancement if a random point on the surface of a sphere is chosen? Figure 1.10 shows a simulation in which 2×10^5 points are randomly selected over one of the spheres in the dimer, the LFIEF is calculated at each point and a histogram (which can be normalized to the total number of points to represent a probability) is created. The most defining characteristic of this result is that the probability of having a certain LFIEF is described by a *power law* at high enhancements (which looks like a ‘line’ on a double logarithmic plot). This is one example of the so-called *long-tail distributions*, and it is a reflection of the fact that the chances of a molecule (distributed at random) to find a hot spot are increasingly rare for the highest enhancements. Moreover, this is directly linked to the strong spatial localization of the hot spot and the fact that they represent a really small fraction of the typical total area available to the molecule.

Examples of long-tail distributions of enhancement at SERS hot spots have been given in the specialized literature (with more sophisticated methods to solve the

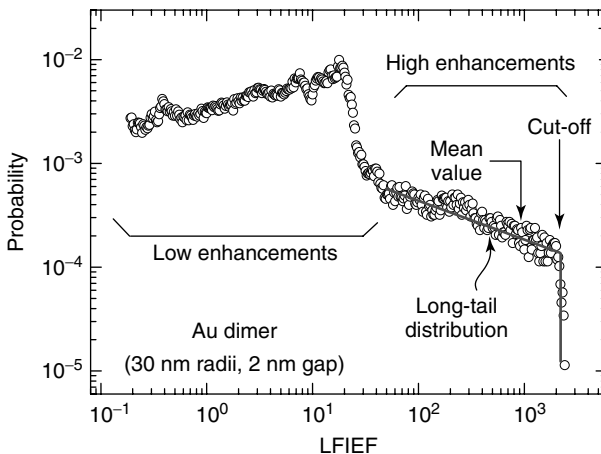


Figure 1.10 Random points on the surface (2×10^5) are chosen for a dimer of Au spheres (30 nm radii) separated by a gap of 2 nm. The LFIEF is obtained in the electrostatic approximation and the histogram displayed here is the resulting distribution (not that it is plotted on a log–log plot). The ‘slope’ in the *high enhancement region* defines a long-tail distribution (with a cut-off at the hot spot) that completely dominates the statistics of LFIEF. All the details of what

happens in the *low enhancement region* can be mostly ignored. Note, for example, that the average value of the enhancement is right towards the end of the tail. Long-tail distributions can also have variances that are larger than the mean! The extreme fluctuations and the dominance of rare events with high enhancements turn out to be a defining property of the SERS enhancement factor (which is linked to the LFIEF).

electromagnetic problem) [45, 49], and here we will only mention that they are fairly universal and always present when hot spots arise. Long-tail distributions have very interesting consequences and produce some extreme statistical characteristics that are a trademark of single-molecule SERS. The topic of the spatial localization of hot spots is therefore central to the understanding of single-molecule SERS statistics, as well as some of its historical contradictions [46, 49].

In the example shown in Figure 1.10, there is a cut-off at the maximum enhancement attainable on the surface, which is right on the main axis joining the two spheres. It is worth mentioning that the tail of the distribution at high enhancements completely dominates the statistics of LFIEFs. For example, Figure 1.10 shows the position of the average LFIEF (mean value) in the distribution. All the details of what happens at low LFIEFs (the region labeled as ‘low enhancements’ in Figure 1.10) are mostly irrelevant. For all practical purposes, we can replace the probability distribution by the effect of the ‘tail’ at high LFIEFs (the region labeled as ‘high enhancements’ in Figure 1.10). More advanced descriptions of these probability distributions have also been studied in the literature [50], to account for the fact that hot spots are imperfect and geometrical parameters vary among certain ranges in real systems. Distributions that do not end abruptly at a cut-off, for example, have been examined and proposed in the literature [50, 51]. Irrespective of their details, the fact remains that the EF distribution amid the presence of hot spots is long-tail and that this a defining property (and a typical feature) of many of the techniques that are associated with the LFIEF, like SERS.

1.4

Electromagnetic Model for the SERS and Fluorescence Enhancement Factors

We are now in a position to address the issue of how much the presence of plasmon resonances affects (enhances or quenches) the Raman or fluorescence signals of molecules. While the main focus of this chapter is on SERS, the mechanism of fluorescence enhancement and quenching is intimately intertwined with it, and it is very useful to understand and highlight the differences. In particular, we can now address the question of what is the connection between the enhancement of Raman and/or fluorescence signals and the LFIEFs discussed in the previous sections.

1.4.1

Enhanced Absorption

The LFIEF represents the increase in intensity a molecule would experience at a specific point with respect to the intensity it would have had in the absence of a metallic nanostructure. Accordingly, all optical magnitudes that depend directly on the intensity are modified (typically enhanced) by the LFIEF. For example, if the molecule absorbs light at a specific wavelength (λ) with a cross section given by σ_{abs} [4], and the field is now affected by an LFIEF, we expect the absorption cross

section to increase to $\text{LFIEF} \times \sigma_{\text{abs}}$; that is, the absorption is LFIEF times the one of the bare molecules. In most of these cases, we talk about LFIEFs that are $\gg 1$ (which are the cases of interest), but we should keep in mind that occasionally the LFIEF can be < 1 (and sometimes even $\ll 1$), in which case it is a *quenching* effect rather than an enhancement. But, if the LFIEF is $\gg 1$, this is equivalent to have the intensity of the incoming light increased at the position of the molecule; hence, the increased absorption.

However, Raman and fluorescence are more complicated optical effects involving at least *two* photons (one taken from the incoming laser beam and the other re-emitted by the molecule) and, moreover, these photons are at different wavelengths. A necessary step to understand the application and use of plasmon resonances in the framework of SERS (or SEF) is, therefore, what the modification of the electromagnetic field does to the efficiency of these processes. It turns out that the effect of the local field enhancement by plasmon resonances is very different for SEF (fluorescence) and SERS (Raman), and it pays off to dwell on the topic shortly and reflect on the two very different scenarios that they present.

1.4.2

Comparison of Raman and Fluorescence Processes

A (Stokes) vibrational Raman scattering event in a molecule is an *instantaneous* optical scattering process in which an incoming photon from the laser at ω_L excites a molecular vibration (with frequency ω_v) while emitting a scattered photon at $\omega_S = (\omega_L - \omega_v)$ [52, 53]. The incident photon does not need to be absorbed and induce electronic transitions in the molecule, since Raman processes are usually excited in the *transparency region* of the optical properties of a molecule (otherwise the process is called *resonance Raman scattering*). In the electronically non-resonant case, it can be considered (from a quantum mechanical point of view) as an interaction with a ‘virtual state’ as depicted in Figure 1.11 [54]. The scattering is *instantaneous* for both photons and they are directly connected through the scattering process. This makes a fundamental difference with fluorescence, for if we ‘enhance’ the rate (photons per unit time) at which inelastically scattered photons (red in Figure 1.11) are produced and detected in the far field (as a Raman signal), we force that increased rate on the incoming (green in Figure 1.11) photons too, and vice versa (i.e. more photons are drawn from the laser).

Fluorescence, on the other hand, is a stepwise process (not instantaneous) that evolves over time through a series of intermediate steps briefly summarized in Figure 1.11 [52, 53]. The initial step involves the absorption of a photon from the ground singlet state S_0 to a state in the vibrational substructure of the first singlet state S_1 . The first ‘leg’ of fluorescence is, therefore, an absorption process. Unlike Raman, the photon must have enough energy to reach S_1 in order to start a fluorescence event and that can only happen for energies above a certain value. This is schematically shown in Figure 1.11a and b. Once the molecule is left in the excited state, it undergoes a series of (rapid) vibrational relaxation processes, reaching (typically) the vibrational ground state of S_1 after a few picoseconds. By

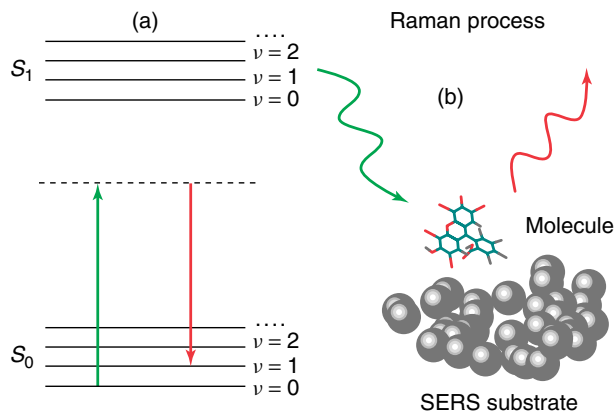


Figure 1.11 A (Stokes) Raman scattering process (under both normal and SERS conditions) is an *instantaneous* process in which the scattered photon is directly linked to the incoming one. The incoming photon does not have to be absorbed at all by the molecule (non-resonant Raman scattering). This is depicted in (a), where a schematic Jablonski diagram for the electronic structure of the molecule is shown.

From a quantum mechanical point of view, the Raman process can be considered as an incoming photon (green) interacting with a ‘virtual state’ (dashed line) and emitting instantaneously a scattered photon (red) that leaves the molecule in an excited vibrational state ($\nu = 1$ in (a)). The same is depicted schematically in (b): both photons are simultaneous and benefit from the enhancement provided by the SERS substrate.

the time the molecule has reached the vibrational ground state of S_1 , it remains there for a few nanoseconds (a typical lifetime before emission for a bare molecule). The main point to realize here is that (unlike Raman) the emission process is now completely independent of the initial absorption; that is, both photons are not linked to each other in a coherent (and instantaneous) way as they are in Raman. For example, if we increase (by some external means) the rate (photons per unit time) at which photons are emitted from the vibrational ground state of S_1 , we cannot *force* more photons per unit time to be absorbed as a result. If one photon has been ‘taken’ from the laser beam to produce a Raman process, then there will be a scattered photon (one cannot exist without the other). In fluorescence, on the contrary, we have situations in which some of the potentially emitted photons (from the ground state of S_1) go ‘missing’ (in non-radiative recombination, for example). Once the molecule is exited to the ground state of S_1 , the best we can do is to recover everything that has been excited in the initial absorption step (in general a fraction will be missing through processes that allow the molecule to relax back to the ground state of S_0 without emitting a photon). But this is independent of the initial absorption process. Therefore, the two processes are effectively ‘disconnected’ in fluorescence (unlike Raman) and this has important consequences for the different way the EFs work in Raman or fluorescence.

One could argue (hopefully without running the risk of straying too much into semantics) that the fluorescence emission (Figure 1.12e and f) has lost the ‘handle’ to control the absorption process (Figure 1.12a and b). Crucial to this

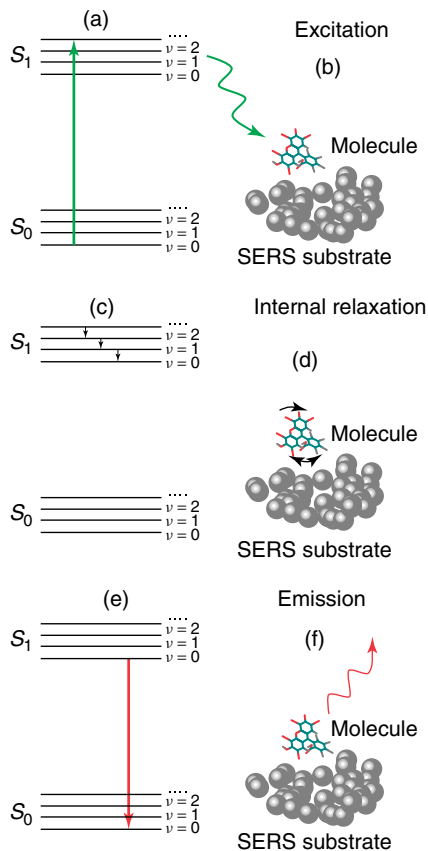


Figure 1.12 A fluorescence process (unlike Raman) can be described as a sequence of events that evolve in time. Fluorescence starts with the absorption of a photon (depicted in (a) and (b)). This process is favoured if the LFIEF is large, resulting in *enhanced absorption*. In (c) and (d), the molecule undergoes vibrational relaxation in the first electronically excited state (S_1). After a certain amount of time (a few

nanoseconds typically), the molecule relaxes to the vibrational levels of the ground state thus emitting a photon (as shown in (e) and (f)). When we increased the rate at which the emission is produced, for example ((e) and (f)), this *did not* force more absorption processes ((a) and (b)) to happen, because the two processes have become disconnected from each other in the relaxation step ((c) and (d)).

‘disconnection’ of the two effects is the vibrational relaxation of the molecule within the electronically excited state S_1 . To summarize these very important points then (for the forthcoming discussion) we can say that both Raman and fluorescence are two photon processes; however, they are fundamentally different from each other: The Raman process is the inelastic scattering of light, while fluorescence involves electronic transitions and, prior to the emission, vibrational relaxation in the electronically excited state. These differences in the microscopic details of two processes will actually result in very different EFs, as we shall see later.

1.4.3

The $|E|^4$ Approximation to SERS Enhancement Factors

Imagine that we have an isolated molecule in which Raman processes are occurring, and we are detecting that as a Raman signal in the far field. Furthermore, imagine now that we put the molecule in an environment where the laser field is enhanced by a certain amount through an LFIEF, such as the ones studied in the previous sections. Evidently, we will produce more Raman processes since, after all, an increase in the LFIEF at ω_L is equivalent to increasing the laser power. We will therefore observe more scattered photons at ω_S . Let us imagine, on the other hand, that we put the molecule in a place that enhances the emitted field at ω_S (Figure 1.11) (in a cavity tuned at ω_S , for example). This will increase the Raman intensity too, for the emission is directly coupled to the excitation and we can always draw more photons from the laser to feed the increased emission rate favoured by the presence of the cavity.

Hence, the Raman process benefits from *both* the emission and excitation enhancements, that is, the LFIEF at both ω_L and ω_S , and this leads to an EF for SERS of the form.⁵⁾

$$\text{EF} = \text{LFIEF}(\omega_L) \times \text{LFIEF}(\omega_S) \quad (1.6)$$

This formula includes a series of implicit approximations, one of which is the fact that it ignores any polarization issues between the incoming and scattered fields. The real Raman process is mediated by a tensor [4, 54], and Equation (1.6) is only an approximation to the real expression of EF [55]. Moreover, further approximations are normally possible. The difference between the LFIEF at ω_L and that at ω_S can sometimes be ignored in many cases. This is due to the fact that $\omega_L - \omega_S$, that is the Raman shift ($\hbar\omega_v = \hbar\omega_L - \hbar\omega_S \sim 0-200$ meV), is sometimes small compared to the typical frequency ranges where the LFIEF shows substantial changes. This is *not* always the case, and there are important cases in SERS where this approximation is actually not valid [56, 57]. But, when it does hold, it provides the simplest possible version of the SERS EF. Taking into account that the LFIEF at a given point is given by Equation (1.2), the SERS EF at r with all the above approximations included reads

$$\text{EF} \sim \text{LFIEF}^2(\omega_L) = \frac{|E(r)|^4}{|E_0(r)|^4} \quad (1.7)$$

This is the so-called $|E|^4$ approximation for the SERS enhancement. Despite its many approximations and simplifications, it provides a very useful yardstick estimate for the actual experimental SERS enhancements in a single molecule located at r . It is also used as a typical figure of merit to evaluate and to compare theoretical models with experiments [45].

We conclude that the EF represented by Equation 1.7 (with all its implicit approximations) represents then a good estimate of the SERS enhancement of a

5) A more rigorous approach using the *optical reciprocity theorem* shows that, indeed, both the incident and emitted photons are

favoured by their respective LFIEFs at the two frequencies.

single molecule. In many experimental situations, however, we measure not one but many molecules that can spread across different places with very different EFs. This is, for example, exemplified in the distribution of the LFIEF in Figure 1.9 close to a hot spot; molecules that differ in position only by a few nanometres can have very different EFs. In such cases, a surface-averaged SERS EF is a more appropriate measure of the overall SERS substrate performance.

Moreover, it is necessary occasionally to reintroduce some of the polarization effects that are washed out in the $|E|^4$ approximation. As a result, a large number of different EFs can be defined for different experimental situations: they all arise ultimately from different averages (over polarization, position, etc.) of the single-molecule EFs. There is not a *single* EF in SERS, but rather several different versions of it. A whole list of different EFs that can be defined for different experimental purposes is given in Ref. [58]. Single-molecule EFs are useful only in some situations (when single molecules are studied!), but there is a natural need to have definitions of the EF that include explicitly the averaging over EFs or orientations. This is particularly true for analytical applications of the technique, which typically imply the measurement of a large number of molecules spread over a substrate with a distribution of EFs according to its geometry and characteristics.

1.4.4

Fluorescence Quenching and Enhancement

Since our emphasis here is on SERS, we shall not dwell into all the details of the fluorescence enhancement, but rather highlight the main points to stress the differences with the SERS case. As stated before, fluorescence begins by an absorption process. The LFIEF at ω_L enhances the intensity of the laser and, therefore, it enhances the absorption. Fluorescence benefits hence from this LFIEF in the initial ‘leg’ of the process (Figure 1.11). For the emission, however, we have a very different situation than that is in SERS. The emission process is ‘disconnected’ from the absorption (it can neither stimulate it nor quench it) because there has been an irreversible interaction (with a concomitant delay time) in the vibrational relaxation process in the excited state S_1 . Therefore, the only possible effect of the environment on the ‘emission leg’ of the process is to modify the decay rate and the relative contribution of radiative to non-radiative decays. This results in a modified quantum yield or *radiative efficiency*. In simple terms, the best we can do on the emission leg is to recover all the possible radiation that the molecule would have emitted. Dyes with a very high quantum yield (which are the majority) have a very high efficiency and produce one photon for each excited molecule to S_1 with a very high efficiency ($\sim 100\%$). In general, however, the presence of a metallic surface nearby provides channels for the absorption of the emitted radiation and the radiation efficiency (η) – related to the modified quantum yield – can be smaller (and sometimes much smaller) than one.

This implies that on the ‘emission leg’ fluorescence can be lost only by the presence of a metal. Combining the effect of enhanced absorption and modified quantum yield, we obtain an EF for fluorescence (for good fluorophores with

intrinsic bare quantum yields $\sim 100\%$) given by

$$EF_{\text{fluor}} \sim \text{LFIEF}(\omega_L)\eta \quad (1.8)$$

where η is the radiation efficiency ($0 \leq \eta \leq 1$). In general, the LFIEF at ω_L will be much larger than one, while the radiation efficiency η can be $\ll 1$ due to non-radiative processes (i.e. emission that ends up absorbed in the metal rather than being radiated to the far field). The competition between the LFIEF in absorption and η is what produces the wide variety of effects observed in the experiments – from fluorescence enhancements (when the LFIEF at the absorption dominates) to fluorescence quenching (where the effect of η is predominant). A more complete description of the SERS and fluorescence EFs has been given in Ref. [4].

1.4.5

Comparison of SERS and Fluorescence Enhancements

At very short distances from the surface (~ 1 nm), most metallic nanostructures will look basically like a ‘plane’ from the point of view of the emitter. The problem of emission close to a plane is well studied in several approximations [4, 59].⁶ Equations 1.7 and 1.8 actually contain all the basic phenomenology observed in SERS probes under *resonant* excitation for typical substrates, to wit:

- Far away from the surface, the fluorescence signal is typically much larger (by many orders of magnitude than the Raman signals, which will be typically swamped in the fluorescence background.
- Closer to the surface (meaning typically ~ 10 nm), there is a mild enhancement of the local field intensity, but the difference between the much more efficient fluorescence process (Figure 1.12) and Raman (Figure 1.11) cannot be compensated; that is, fluorescence may be enhanced (SEF regime) and will again completely dominate the spectrum.
- At much closer distances (a few nanometers), Raman begins benefiting from higher enhancements at both the incoming and outgoing frequencies, while the emission leg of the fluorescence begins experiencing the effect of a reduced η . Even though fluorescence benefits from the increased LFIEF at the incoming field (enhanced absorption), the condition $\eta \ll 1$ starts to dominate and the fluorescence appears as ‘partially quenched’. In this regime, the Raman (SERS) signals begin to ‘pop out’ above the fluorescence background. Both SERS and SEF are observed.
- At really short distances from the surface (~ 1 nm), the quenching of the fluorescence emission due to η is really effective, and fluorescence may disappear from the spectrum. It is important to realize that this does not mean that the molecule itself is not fluorescing, but rather that its emission is being mainly

6) At very short distances (d) from a surface the non-radiative components of the emission scale like $\sim 1/d^3$. Therefore, at sufficiently close distances from the surface (subject

to the geometrical constraints imposed by the molecular size and shape of the chromophore) the fluorescence emission can always be quenched.

channelled into non-radiative processes in the metal. At the same time, the Raman process observed in the far field is still benefiting from the LFIEF at both the excitation and emission wavelengths. Accordingly, this is the regime where Raman (SERS) signals dominate and fluorescence is quenched. It is worth highlighting, however, that a residual fluorescence signal may still be present, albeit strongly spectrally modified, and this can then be the origin of the so-called SERS continuum in resonant conditions [20]. The case when the laser excitation wavelength is not only in resonance with the plasmonic substrate but also with an electronic absorption of the adsorbed molecule is called surface-enhanced resonance Raman scattering (SERRS; see also Chapters 10 and 11).

Most of the phenomenologies observed in SERS and SEF under the presence of plasmon resonances is actually contained in combinations of the above given situations, and this is schematically displayed in Figure 1.13.

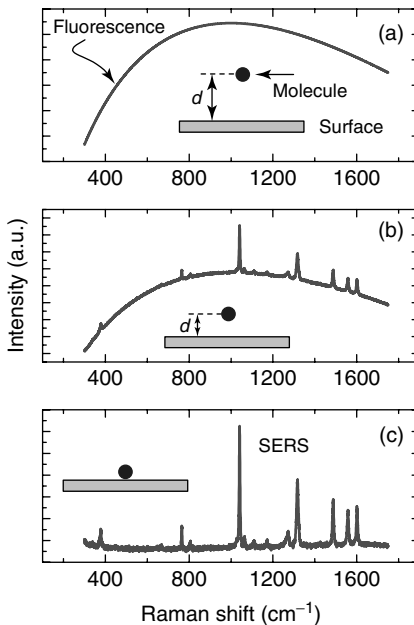


Figure 1.13 Schematic representation of the relative intensities of fluorescence and SERS for molecules at different distances from a metallic surface. We assume the case of a resonant excitation of a dye that produces fluorescence under normal conditions at the chosen laser wavelength. In (a) the molecule is far away from the surface and fluorescence dominates. In (b), the molecule has come closer to the surface and the LFIEF increases. SERS benefits from the higher LFIEF, and fluorescence (even when it

is benefiting from the higher LFIEF at the absorption leg of the process) begins experiencing the quenching of the radiative efficiency η . In (c), the molecule has come even closer to the surface and the fluorescence has been quenched, thus revealing the SERS spectrum which is at its maximum efficiency. Note that this does *not* imply that the molecule is not fluorescing, but rather that the emission is quenched (i.e. η dominates).

The ‘competition’ between the efficiencies of both processes refers here to spectrally integrated magnitudes (the total spectrally integrated amount of fluorescence or the integrated signal of a Raman peak). Additionally, if we look at the spectral domain (i.e. not only the overall intensity but also the shape of the spectrum), there are other phenomena that arise besides the general phenomenology described above such as *spectrally modified fluorescence* [20]. These are, however, more advanced topics that can be introduced in a second stage and are very case dependent.

1.4.6

Other Forms of Enhancements

Besides the electromagnetic enhancement based on plasmon resonances (described up to here in this chapter), there are other known forms of enhancements in SERS, which are normally grouped under the general denomination of ‘chemical enhancement’ [60–63]. The EFs described so far in this chapter (all linked in one way or another to the LFIEF) would exist even if the molecule were not there at all! They are an intrinsic electromagnetic property of the substrate, not the analyte. But once the molecule is introduced into the problem, its simultaneous interaction with the metal and the electromagnetic field can induce additional contributions to the SERS enhancement. The existence of chemical enhancements is well established and documented since the early days of SERS [2]. It is normally divided into different categories depending on the strength of the interaction between the electronic structure of the molecule and that of the metal [4, 60]. It can contain, in addition, a number of very interesting and complex aspects, such as photo-induced electron transfer between the molecule and the metal [61] or the subtler effects of ionic species (in particular, chlorine [62]). From the standpoint of this introduction, we only mention its existence and refer the reader to the more specialized literature for further details [4]. An important point to highlight, however, is the fact that in all known SERS cases the chemical contribution to the enhancement can only account for an additional factor of ~ 10 (in the best of cases). Standard SERS EFs in the wide range of $\sim 10^3$ – 10^{10} are, hence, primarily electromagnetic in nature and produced by surface plasmon resonances in metals (of the kind described in this chapter). SERS – as we know it – would not exist if the chemical enhancement were the only source boosting the signals. The chemical enhancement plays a crucial role in the understanding of the finer details of the effect and in its basic science. But, any realistic application of the technique to boost the Raman signals will always start by tailoring the electromagnetic enhancements through surface plasmon resonances in different geometries and configurations [64, 65]. It is only now that the ever-increasing power of computers has also started to unveil some of the details pertaining to the electronic interaction of molecules with metals [63]; the ultimate microscopic source of the chemical enhancement.

1.5

The Magnitude of the SERS Enhancement Factor in Typical Cases

Before concluding, a brief comment is appropriate on the magnitude of the EF observed experimentally under different conditions. This has been, in fact, a contentious issue for a very long time in SERS, and a topic that has been plagued for many years by experimental uncertainties and diverging views [45, 58]. As mentioned earlier, part of the problem is that there is a myriad of different EFs that one can define (spatially averaged, polarization averaged, etc.). But, this is only part of the problem, for some of the issues relate to different experimental practices and lack of consensus on how to actually measure the EFs. We shall not dwell here on all the various details of the problem, which have been thoroughly studied in Ref. [58] and further expanded in Ref. [4]. We shall concentrate, however, on the ‘simplest’ case: single-molecule EFs in SERS.

When we are measuring a single molecule, we are in a situation in which many of the uncertainties of *spatial* averaging (the fact that molecules at different positions experience different enhancements) are ruled out. There are still a few pending issues that can affect the definition of the EF (or what is actually being measured) such as surface selection rules [66, 67]. We only mention here that of all possible cases related to the quantification of SERS EFs, the single-molecule case poses the simplest one with the smallest number of assumptions. Needless to say, the price is paid here in a different way: through the experimental challenge of making sure that we are actually measuring *one* molecule. The rest of the task is to be able to normalize the signal coming from a single molecule with respect to a (non-SERS) spectrum of a reference compound with a known Raman differential cross section. But the latter is a relatively simpler experimental procedure, and the real difficulty lies in making sure that single molecules are indeed being observed reliably.

It is a relatively recent development though [58] that SERS EFs have been quantified and measured with techniques that allow the identification of single-molecule cases. The conditions needed to ensure that the SERS signals we are measuring come from single-molecules can be achieved through a variety of methods (Langmuir–Blodgett films [68–71], TERS [33–35], and bi-analyte SERS [5, 72–74]), but direct quantifications of single-molecule SERS cross sections and EFs have been done almost exclusively with the bi-analyte SERS method [58, 72]. Several situations of single-molecule EFs have been considered in the literature, including the possible effects of photobleaching [51] (which limits the maximum observed EFs [75]). What follows is a very brief (and, accordingly, necessarily incomplete) description of the main experimental findings to date:

- Single-molecule SERS EFs up to a maximum value of $\sim 10^{10}$ [76] have been observed in many different experimental conditions. The minimum value to observe single molecules is around $\sim 10^7$ – 10^8 for resonant or pre-resonant molecules, and even though these values are strongly dependent on the exact experimental conditions [45] the fact remains that they are (at least) up to a million times smaller than what was originally thought to be necessary to observe single molecules in SERS. These enhancements are in perfect accord

with what is expected theoretically from electromagnetic calculations (in the $|E|^4$ approximation, for example).

- For cases involving many molecules, the EF is invariably an average over the different situations of the individual molecules over the substrate. Average EFs play an important role in applications, even if their microscopic origin is obscured by the averaging process. But they provide sometimes the only mean to compare the performance of different substrates. For non-optimized conditions, average EFs for SERS can be as low as $\sim 10^{-3}$. More typical values for useful applications will be in the range of $\sim 10^4$ – 10^6 , and these values should be considered standard for the technique.

Enhancements in the range 10^7 – 10^{10} are obtained in many situations and can easily provide single-molecule sensitivity (including cases of non-resonant molecules [76]). These latter cases appear more often in ‘disordered’ substrates, where it is difficult to control the geometrical parameters of the problem and we rely solely on ‘accidental’ formation of hot spots. An alternative to produce hot spots with EFs in this range (in a controlled manner) is the TERS described earlier [33–35], albeit with the proviso in mind that it is very difficult to position the molecule at the right place. The vast majority of single-molecule SERS experiments is performed in disordered substrates and relies heavily on the statistics of events. There is, nevertheless, an increasing number of single-molecule experiments with TERS, but reliable values for the actual EFs that are achieved have not yet appeared in the literature. The ‘normalization’ procedure (with respect to a reference compound of known differential cross section) using TERS is a lot more difficult.

A brief comment on our actual experimental ability to control the EF is opportune at this stage. The more our desire to control the EF, the more it becomes necessary to control the geometrical aspects of the problem at the nanoscale. This is particularly true for high enhancements, which normally come from coupled plasmon resonances at gaps (as shown in Figure 1.9) with typical dimensions ~ 1 – 2 nm. This has been informally dubbed ‘the SERS uncertainty principle’ by Natan [77], in the sense that the higher the enhancement we desire, the more uncontrollable the geometrical variables of the problem become (from an experimental point of view). While this is merely a figure of speech (and not an actual principle), it does highlight the fact that highest possible enhancements are always limited by our ability to control the nanoscale world to a precision comparable to molecular dimensions (~ 1 nm).

1.6 Conclusions

We hope that somebody who has not heard about plasmon resonances and SERS/SEF enhancements before would have obtained at this stage a clear idea of the basic concepts underlying the EF in SERS and fluorescence, at least at a qualitative level. *Shape, size and interactions* are at the heart of the immensely

rich and complex optical response of metallic nanostructures and the stunning variety of optical phenomena that arise in plasmonics. Needless to say, a much deeper understanding of the details of the electromagnetic response of metallic nanostructures requires dwelling on the details of the solutions and the multitude of analytical and numerical methods to obtain them. While this is left to more specialized literature [4], we believe that a very basic conceptual understanding can be obtained through the topics highlighted in this chapter. More advanced theoretical concepts on the theory of plasmon resonances can be obtained from Ref. [78], or from a more SERS-oriented point of view in Refs. [3, 4].

References

1. Moskovits, M. (1985) Surface-enhanced spectroscopy. *Rev. Mod. Phys.*, **57**, 783–826.
2. Otto A. (1984) Surface enhanced Raman scattering: classical and chemical origins, in *Light Scattering in Solids IV*, Topics in Applied Physics, vol. 103 (eds M. Cardona. and G. Guntherodt.), Springer, Berlin, pp. 289–418.
3. Aroca, R. (2006) *Surface Enhanced Vibrational Spectroscopy*, Wiley, Chichester.
4. Le Ru, E.C. and Etchegoin, P.G. (2009) *Principles of Surface-enhanced Raman Spectroscopy and Related Plasmonic Effects*, Elsevier, Amsterdam.
5. Goulet, P.J.G. and Aroca, R.F. (2007) Distinguishing individual vibrational fingerprints: single-molecule surface-enhanced resonance Raman scattering from one-to-one binary mixtures in Langmuir-Blodgett monolayers. *Anal. Chem.*, **79**, 2728–2734.
6. McCabe, A.F., Eliasson, C., Prasath, R.A. *et al.* (2006) SERRS labeled beads for multiplex detection. *Faraday Discuss.*, **132**, 303–308.
7. Smith, W.E. (2008) Practical understanding and use of surface enhanced Raman scattering/surface enhanced resonance Raman scattering in chemical and biological analysis. *Chem. Soc. Rev.*, **37**, 955–964.
8. Lyandres, O., Shah, N.C., Yonzon, C.R. *et al.* (2005) Real-time glucose sensing by surface-enhanced Raman spectroscopy in bovine plasma facilitated by a mixed decanethiol/mercaptohexanol partition layer. *Anal. Chem.*, **77**, 6134–6139.
9. Faulds, K., Barbagallo, R.P., Keer, J.T. *et al.* (2004) SERRS as a more sensitive technique for the detection of labelled oligonucleotides compared to fluorescence. *Analyst*, **129**, 567–568.
10. Sabatte, G., Keir, R., Lawlor, M. *et al.* (2008) Comparison of surface-enhanced resonance Raman scattering and fluorescence for detection of a labeled antibody. *Anal. Chem.*, **80**, 2351–2356.
11. Koo, T.W., Chan, S., Sun, L. *et al.* (2004) Specific chemical effects on surface-enhanced Raman spectroscopy for ultra-sensitive detection of biological molecules. *Appl. Spectrosc.*, **58**, 1401–1407.
12. Vo-Dinh, T., Allain, L.R. and Stokes, D.L. (2002) Cancer gene detection using surface-enhanced Raman scattering (SERS). *J. Raman Spectrosc.*, **33**, 511–516.
13. Haynes, C.L., Yonzon, C.R., Zhang, X. and Van Duyne, R.P. (2005) Surface enhanced Raman sensors: early history and the development of sensors for quantitative biowarfare agent and glucose detection. *J. Raman Spectrosc.*, **36**, 471–484.
14. Sägmüller, B., Schwarze, B., Brehm, G. and Schneider, S. (2001) Application of SERS spectroscopy to the identification of (3,4-methylenedioxy)amphetamine in forensic samples utilizing matrix stabilized silver halides. *Analyst*, **126**, 2066–2071.
15. Chen, K., Leona, M., Vo-Dinh, K.C. *et al.* (2006) Application of surface-enhanced Raman scattering (SERS) for the identification of anthraquinone dyes used

- in works of art. *J. Raman Spectrosc.*, **37**, 520–527.
16. Centeno, S.A. and Shamir, J. (2008) Surface enhanced Raman scattering (SERS) and FTIR characterization of the sepia melanin pigment used in works of art. *J. Mol. Struct.*, **873**, 149–159.
 17. Chen, K., Leona, M. and Vo-Dinh, T. (2007) Surface-enhanced Raman scattering for identification of organic pigments and dyes in works of art and cultural heritage material. *Sens. Rev.*, **27**, 109–120.
 18. Dulkeith, E., Morteani, A.C., Niedereichholz, T. *et al.* (2002) Fluorescence quenching of dye molecules near gold nanoparticles: radiative and nonradiative effects. *Phys. Rev. Lett.*, **89**, 203002–203005.
 19. Lakowicz, J.R. (2005) Radiative decay engineering 5: metal-enhanced fluorescence and plasmon emission. *Anal. Biochem.*, **337**, 171–194.
 20. Le Ru, E.C., Etchegoin, P.G., Grand, J. *et al.* (2007) The mechanisms of spectral profile modification in surface enhanced fluorescence. *J. Phys. Chem. C*, **44**, 16076–16079.
 21. Haes, A.J. and Van Duyne, R.P. (2005) A unified view of propagating and localized surface plasmon resonance biosensors. *Anal. Bioanal. Chem.*, **379**, 920–930.
 22. Zayatsa, A.V., Smolyaninov, I.I. and Maradudin, A.A. (2005) Nano-optics of surface plasmon polaritons. *Phys. Rep.*, **408**, 131–314. (and references therein).
 23. Novotny L. (2000) Forces in optical near-fields, in *Near-field Optics and Surface Plasmon Polaritons, Topics in Applied Physics*, vol. 81 (ed. S. Kawata.), Springer-Verlag, Berlin, pp. 123–141.
 24. Born, M. and Wolf, E. (1999) *Principles of Optics*, Cambridge University Press, Cambridge.
 25. Madelung, O. (1978) *Introduction to Solid-State Theory*, Springer-Verlag, Berlin.
 26. Kittel, C. (1986) *Introduction to Solid State Physics*, John Wiley & Sons, Inc, New York.
 27. Etchegoin, P.G., Le Ru, E.C. and Meyer, M. (2006) An analytic model for the optical properties of gold. *J. Chem. Phys.*, **125**, 164705–164707.
 28. Griffiths, D.J. (1999) *Introduction to Electrodynamics*, Prentice Hall, New Jersey.
 29. Jackson, J.D. (1998) *Classical Electrodynamics*, Wiley, New York.
 30. Rojas, R. and Claro, F. (1993) Theory of surface enhanced Raman-scattering in colloids. *J. Chem. Phys.*, **98**, 998–1006.
 31. Prodan, E., Radloff, C., Halas, N.J. and Nordlander, P. (2003) A hybridization model for the plasmon response of complex nanostructures. *Science*, **302**, 419–422.
 32. Etchegoin, P., Cohen, L.F., Hartigan, H. *et al.* (2003) Electromagnetic contribution to surface enhanced Raman scattering revisited. *J. Chem. Phys.*, **119**, 5281–5289.
 33. Pettinger, B., Picardi, G., Schuster, R. and Ertl, G. (2002) Surface-enhanced and STM-tip-enhanced Raman spectroscopy at metal surfaces. *Single Mol.*, **5** (6), 285–294.
 34. Pettinger, B., Ren, B., Picardi, G. *et al.* (2005) Tip-enhanced Raman spectroscopy (TERS) of malachite green isothiocyanate at Au(111): bleaching behavior under the influence of high electromagnetic fields. *J. Raman Spectrosc.*, **36**, 541–550.
 35. Steidtner, J. and Pettinger, B. (2008) Tip-enhanced Raman spectroscopy and microscopy on single dye molecules with 15 nm resolution. *Phys. Rev. Lett.*, **100**, 236101–236104.
 36. Anderson, M.S. and Pike, W.T. (2002) A Raman-atomic force microscope for apertureless-near-field spectroscopy and optical trapping. *Rev. Sci. Instrum.*, **73**, 1198–1203.
 37. Downes, A., Salter, D. and Elfick, A. (2006) Finite element simulations of tip-enhanced Raman and fluorescence spectroscopy. *J. Phys. Chem. B*, **110**, 6692–6698.
 38. Ward, D.R., Halas, N.J., Cizsek, J.W. *et al.* (2008) Simultaneous measurements of electronic conduction and Raman response in molecular junctions. *Nano Lett.*, **8**, 919–924.
 39. Hudson, S.D. and Chumanov, G. (2009) Bioanalytical applications of SERS

- (surface-enhanced Raman spectroscopy). *Anal. Bioanal. Chem.*, **394**, 679–686.
40. Vial, A. (2007) Implementation of the critical points model in the recursive convolution method for modeling dispersive media with the finite-difference time domain method. *J. Opt. A: Pure Appl. Opt.*, **9**, 745–748. (and references therein).
 41. (1985) *Handbook of Optical Constants of Solids* (ed. E.D. Palik.), Academic Press.
 42. Tian, Z.Q., Ren, B. and Wu, D.Y. (2002) Surface-enhanced Raman scattering: from noble to transition metals and from rough surfaces to ordered nanostructures. *J. Phys. Chem. B*, **106**, 9463–9483.
 43. Tian, Z.Q., Gao, J.S., Li, X.Q. *et al.* (1998) Can surface Raman spectroscopy be a general technique for surface science and electrochemistry? *J. Raman Spectrosc.*, **29**, 703–711.
 44. Tian, Z.Q. and Ren, B. (2004) Adsorption and reaction at electrochemical interfaces as probed by Surface-Enhanced Raman Spectroscopy. *Annu. Rev. Phys. Chem.*, **55**, 197–229.
 45. Etchegoin, P.G. and Le Ru, E.C. (2008) A perspective on single molecule SERS: current status and future challenges. *Phys. Chem. Chem. Phys.*, **10**, 6079–6089.
 46. Etchegoin, P.G., Meyer, M. and Le Ru, E.C. (2007) Statistics of single molecule SERS signals: is there a Poisson distribution of intensities? *Phys. Chem. Chem. Phys.*, **9**, 3006–3010.
 47. Nie, S. and Emory, S.R. (1997) Probing single molecules and single nanoparticles by surface-enhanced Raman scattering. *Science*, **275**, 1102–1106.
 48. Kneipp, K., Wang, Y., Kneipp, H. *et al.* (1997) Single molecule detection using surface-enhanced Raman scattering (SERS). *Phys. Rev. Lett.*, **78**, 1667–1670.
 49. Le Ru, E.C., Etchegoin, P.G. and Meyer, M. (2006) Enhancement factor distribution around a single surface-enhanced Raman scattering hot spot and its relation to single molecule detection. *J. Chem. Phys.*, **125**, 204701–204714.
 50. Le Ru, E.C. and Etchegoin, P.G. (2009) Phenomenological local field enhancement factor distributions around electromagnetic hot spots. *J. Chem. Phys.*, **130**, 181101–181104.
 51. Fang, Y., Seong, N.-H. and Dlott, D.D. (2008) Measurement of the distribution of site enhancements in surface-enhanced Raman scattering. *Science*, **321**, 388–392.
 52. Haken, H., Wolf, H.C. and Brewer, W.D. (2004) *Molecular Physics and Elements of Quantum Chemistry: Introduction to Experiments and Theory*. Springer-Verlag, Berlin.
 53. Demtröder, W. (2002) *Laser Spectroscopy*. Springer-Verlag, Berlin.
 54. Long, D.A. (2002) *The Raman Effect, A Unified Treatment of the Theory of Raman Scattering by Molecules*. John Wiley & Sons, Ltd, Chichester.
 55. Le Ru, E.C. and Etchegoin, P.G. (2006) Rigorous justification of the $|E|^4$ enhancement factor in surface enhanced Raman spectroscopy. *Chem. Phys. Lett.*, **423**, 63–66.
 56. Le Ru, E.C., Etchegoin, P.G., Grand, J. *et al.* (2008) Surface enhanced Raman spectroscopy on nanolithography-prepared substrates. *Curr. Appl. Phys.*, **8**, 467–470.
 57. Le Ru, E.C., Grand, J., Félijd, N. *et al.* (2008) Experimental verification of the SERS electromagnetic model beyond the $|E|^4$ approximation: polarization effects. **112**, 8117–8121.
 58. Le Ru, E.C., Blackie, E., Meyer, M. and Etchegoin, P.G. (2007) SERS enhancement factors: a comprehensive study. *J. Phys. Chem. C*, **111**, 13794–13803.
 59. Ford, G.W. and Weber, W.H. (1984) Electromagnetic interactions of molecules with metal surfaces. *Phys. Rep.*, **113**, 195–287.
 60. Tian, Z.Q. (2006) General discussions section. *Faraday Discuss.*, **132**, 309–319.
 61. Xie, Y., Wu, D.Y., Liu, G.K. *et al.* (2003) Surface-enhanced Raman scattering study of the surface coordination of porphyrins adsorbed on silver. *J. Electroanal. Chem.*, **554**, 417–420.
 62. Otto, A., Bruckbauer, A. and Chen, Y.X. (2003) On the chloride activation in

- SERS and single molecule SERS. *J. Mol. Struct.*, **661**, 501–514.
63. Wu, D.Y., Duan, S., Ren, B. and Tian, Z.Q. (2005) Density functional theory study of surface-enhanced Raman scattering spectra of pyridine adsorbed on noble and transition metal surfaces. *J. Raman Spectrosc.*, **36**, 533–540.
 64. Banholzer, M.J., Millstone, J.E., Quin, L. and Mirkin, C.A. (2008) Rationally designed nanostructures for surface-enhanced Raman spectroscopy. *Chem. Soc. Rev.*, **37**, 885–897.
 65. Lal, S., Grady, N.K., Kundu, J. *et al.* (2008) Tailoring plasmonics substrates for surface-enhanced spectroscopies. *Chem. Soc. Rev.*, **37**, 898–911.
 66. Moskovits, M. (1982) Surface selection rules. *J. Chem. Phys.*, **77**, 4408–4416.
 67. Le Ru, E.C., Meyer, M., Blackie, E. and Etchegoin, P.G. (2008) Advanced aspects of electromagnetic SERS enhancement factors at a hot-spot. *J. Raman Spectrosc.*, **39**, 1127–1134.
 68. Pieczonka, N.P.W. and Aroca, R.F. (2008) Single molecule analysis by surface-enhanced Raman scattering. *Chem. Soc. Rev.*, **37**, 946–954.
 69. Constantino, C.J.L., Lemma, T., Antunes, P.A. and Aroca, R. (2001) Single-molecule detection using surface-enhanced resonance Raman scattering and Langmuir-Blodgett monolayers. *Anal. Chem.*, **73**, 3674–3678.
 70. Goulet, P.J.G., Pieczonka, N.P.W. and Aroca, R.F. (2005) Mapping single-molecule SERS from Langmuir-Blodgett monolayers on nanostructured silver island films. *J. Raman Spectrosc.*, **36**, 574–580.
 71. Goulet, P.J.G., Pieczonka, N.P.W. and Aroca, R.F. (2003) Overtones and combinations of single-molecule surface-enhanced resonance Raman scattering spectra. *Anal. Chem.*, **75**, 1918–1923.
 72. Le Ru, E.C., Meyer, M. and Etchegoin, P.G. (2006) Proof of single-molecule sensitivity in surface enhanced Raman scattering (SERS) by means of a two-analyte technique. *J. Phys. Chem. B*, **110**, 1944–1948.
 73. Dieringer, J.A., Lettan II, R.B., Scheidt, K.A. and Van Duyne, R.P. (2007) A frequency domain existence proof of single-molecule surface-enhanced Raman spectroscopy. *J. Am. Chem. Soc.*, **129**, 16249–16256.
 74. Blackie, E., Le Ru, E.C., Meyer, M. *et al.* (2008) Bi-analyte SERS with isotopically edited dyes. *Phys. Chem. Chem. Phys.*, **10**, 4147–4153.
 75. Etchegoin, P.G., Lacharmoise, P.D. and Le Ru, E.C. (2009) Influence of photostability on single-molecule surface enhanced Raman scattering enhancement factors. *Anal. Chem.*, **81**, 682–688.
 76. Blackie, E.J., Le Ru, E.C. and Etchegoin, P.G. (2009) Single-molecule surface-enhanced Raman spectroscopy of nonresonant molecules. *J. Am. Chem. Soc.*, **131**, 14466–14472.
 77. Natan, M.J. (2006) Concluding remarks: surface enhanced Raman scattering. *Faraday Discuss.*, **132**, 321–328.
 78. Novotny, L. and Hecht, B. (2006) *Principles of Nano-optics*, Cambridge University Press, Cambridge.

